Biomedicine & Pharmacotherapy 190 (2025) 118434

Contents lists available at ScienceDirect

Biomedicine & Pharmacotherapy

journal homepage: www.elsevier.com/locate/biopha

Vinpocetine alleviates chemotherapy-induced peripheral neuropathy by reducing oxidative stress and enhancing mitochondrial biogenesis in mice

Guanghai Nan [a,b], Lin Lin [c], Leejeong Kim [a], Kyeongmin Kim [a], Nari Kang [a], Hee Young Kim [a,b,e], Myeounghoon Cha [a,d,*], Bae Hwan Lee [a,b,e,**]

[a] Department of Physiology, Yonsei University College of Medicine, Seoul 03722, Republic of Korea
[b] Graduate School of Medical Science, Brain Korea 21 Project, Yonsei University College of Medicine, Seoul 03722, Republic of Korea
[c] Department of Anesthesiology and Pain Medicine, Anesthesia and Pain Research Institute, Yonsei University College of Medicine, Seoul 03722, Republic of Korea
[d] Department of Physiology, College of Medicine, Soonchunhyang University, Cheonan 31151, Republic of Korea
[e] Brain Research Institute, Yonsei University College of Medicine, Seoul 03722, Republic of Korea

ARTICLE INFO

Keywords:
Chemotherapy-induced peripheral neuropathy
Vinpocetine
Mitochondrial biogenesis
Oxidative stress
Neuronal hyperexcitability
Central sensitization

ABSTRACT

Chemotherapy-induced peripheral neuropathy (CIPN) is a major dose-limiting side effect of cancer treatment and is primarily driven by oxidative stress and mitochondrial dysfunction. Despite its clinical relevance, effective mechanism-based therapies remain limited. Vinpocetine, a neuroprotective compound, has shown antioxidant, anti-inflammatory, and mitochondrial function-preserving effects; however, its efficacy in CIPN remains unknown. This study aimed to evaluate the efficacy and underlying mechanisms of vinpocetine in a paclitaxel-induced CIPN mouse model. In behavioral tests, acute administration of vinpocetine alleviated mechanical hypersensitivity, whereas repeated treatment provided sustained relief from mechanical, thermal, and cold hypersensitivity. Mechanistically, vinpocetine reduced mitochondrial reactive oxygen species (ROS), restored SOD2 levels, and activated mitochondrial biogenesis via the PGC-1α-NRF1-TFAM pathway, as shown by Western blot analysis. In oxidative stress-induced pain models, vinpocetine also attenuated mechanical hypersensitivity, reinforcing its antioxidant properties. Voltage-sensitive dye imaging revealed reduced spinal neuronal hyperexcitability. Immunohistochemistry analysis further demonstrated reduced expression of AMPA and PKC-α in NeuN-positive neurons. This preclinical study is the first to demonstrate that vinpocetine alleviates CIPN by enhancing mitochondrial biogenesis, reducing oxidative stress, and suppressing neuronal excitability in the spinal cord. These results provide mechanistic insights into its effects on CIPN and support further translational research in this indication.

1. Introduction

Chemotherapy-induced peripheral neuropathy (CIPN) is a common and often debilitating adverse effect of chemotherapeutic agents such as platinum-based drugs, taxanes, and vinca alkaloids [1,2]. Approximately 68 % of patients develop CIPN during the first month of treatment, and approximately 30 % experience symptoms that persist beyond six months [3]. These symptoms, including numbness, tingling, burning pain, and motor impairment, typically follow a bilateral 'glove-and--stocking' distribution [4,5]. CIPN significantly reduces patient quality of life and frequently leads to dose reduction or treatment discontinuation, ultimately compromising therapeutic efficacy [6–8]. Although the serotonin-noradrenaline reuptake inhibitor, duloxetine, is the only treatment with moderate clinical recommendation, its efficacy remains limited, and other symptomatic options offer inconsistent relief or poor tolerability [9–11]. These limitations underscore the urgent need for mechanism-based therapeutic strategies [12].

Recent studies have identified oxidative stress and mitochondrial dysfunction in the spinal cord as the central contributors to CIPN pathogenesis [13,14]. Chemotherapeutic agents promote the excessive generation of reactive oxygen species (ROS), which impair antioxidant defenses and disrupt mitochondrial function [15,16]. This leads to ATP

* Correspondence to: Department of Physiology, College of Medicine, Soonchunhyang University, 31 Soonchunhyang6-gil, Dongnam-gu, Cheonan-si, Chungcheongnam-do 31151, Republic of Korea.
** Correspondence to: Department of Physiology, Yonsei University College of Medicine, 50-1, Yonsei-ro, Seodaemun-gu, Seoul 03722, Republic of Korea.
E-mail addresses: mcha@sch.ac.kr (M. Cha), bhlee@yuhs.ac (B.H. Lee).

https://doi.org/10.1016/j.biopha.2025.118434
Received 6 June 2025; Received in revised form 22 July 2025; Accepted 1 August 2025
Available online 6 August 2025

depletion and increases neuronal excitability [17–19]. Consistent with this mechanism, paclitaxel-induced pain models show sensory neurons with swollen and vacuolated mitochondria, further supporting the link between mitochondrial injury and neuropathic symptoms [20].

Mitochondrial dysfunction is further exacerbated by the suppression of mitochondrial biogenesis, particularly through the downregulation of peroxisome proliferator-activated receptor gamma coactivator-1α (PGC-1α), which is a central regulator of mitochondrial renewal and antioxidant enzyme expression [21–23]. Decreased PGC-1α impairs the expression of protective factors, such as superoxide dismutase 2 (SOD2) and uncoupling protein 2 (UCP2), amplifying redox imbalance and neuronal energy failure [21]. This contributes to synaptic hyperexcitability and central sensitization [24,25]. In CIPN models, PGC-1α expression is markedly reduced, suggesting that impaired mitochondrial biogenesis aggravates mitochondrial damage and oxidative stress [26]. Therefore, enhancing PGC-1α activity may improve mitochondrial function and alleviate oxidative stress in CIPN.

Considering the importance of oxidative stress and impaired PGC-1α-mediated mitochondrial biogenesis in CIPN, there is an urgent need for therapeutics targeting these upstream mechanisms. Rather than relying solely on traditional antioxidants with limited translational success, agents capable of modulating mitochondrial regulatory pathways have the potential to provide more effective and sustainable benefits [27,28]. Vinpocetine, which is known for its regulatory effects on oxidative stress and mitochondrial function, is a promising candidate, although its potential in CIPN has not been systematically evaluated.

Vinpocetine, a synthetic derivative of the vinca alkaloid vincamine, is widely prescribed for cerebrovascular and neurodegenerative disorders owing to its neuroprotective properties [29–32]. It exerts analgesic efficacy in models of inflammatory and visceral pain and alleviates pain by enhancing endogenous antioxidant defenses [32–34]. In vitro, vinpocetine improves mitochondrial function, suggesting its potential relevance in CIPN [35]. However, its in vivo effects on mitochondrial function in CIPN, particularly on oxidative stress and spinal mechanisms, remain unclear.

This study investigated whether vinpocetine alleviates paclitaxel-induced CIPN by enhancing mitochondrial biogenesis, reducing oxidative stress, and modulating spinal neuronal hyperexcitability. To this end, we employed behavioral, molecular, and imaging approaches to assess its effects on mitochondrial ROS, biogenesis-related pathways, and spinal excitability.

2. Materials and methods

2.1. Experimental animals

Adult male C57BL/6 mice (6 weeks; 20–22 g; Orient Bio, Sungnam, Gyonggi, South Korea) were used for experiments in this study. Mice were housed in groups of five with sawdust bedding in a climate-controlled environment with a 12-hour light/dark cycle. The laboratory diet was available *ad libitum* except when the mice were being tested. Animals were allowed to acclimate for at least 7 days after arrival at the Association for Assessment and Accreditation of Laboratory Animal Care (AAALAC)-accredited Yonsei University College of Medicine Animal Care Facilities. All animal procedures adhered to the National Institutes of Health (NIH) guidelines and were approved by the Institutional Animal Care and Use Committee (IACUC) of Yonsei University Health System (permit no.: 2023–0010).

Mice were randomly assigned to treatment groups using a computer-generated randomization list. Sample sizes (n = 6–10 per group) were based on prior CIPN studies and were confirmed to be statistically adequate for detecting large effects across behavioral, molecular, and histological experiments. Only male mice were used to avoid variability due to the estrous cycle, which may influence pain sensitivity.

2.2. Chemotherapy-induced peripheral neuropathy model

Paclitaxel (T7402, Sigma-Aldrich, St. Louis, MO, USA) was used to establish the CIPN model. It was prepared at 25 mg/mL in a mixture of 50 % Cremophor® EL and 50 % anhydrous ethanol and stored in a deep freezer until use. The stock solution was diluted with 0.9 % sterile saline immediately before injection. Mice were injected intraperitoneally (i.p.) with paclitaxel on four alternate days, designated as post-injection days (PID) 0, 2, 4, and 6, at a dose of 2 mg/kg per injection.

2.3. Drug administration

To evaluate the analgesic and antioxidant effects of vinpocetine (V6383, Sigma-Aldrich), it was dissolved in dimethyl sulfoxide (DMSO) and diluted with 0.9 % sterile saline immediately before administration. The control group received an equivalent volume of DMSO mixed with sterile saline. For intraperitoneal injection, vinpocetine was administered at different dosages: 2.5 mg/kg, 5 mg/kg, 10 mg/kg, and 20 mg/kg, with the injection volume adjusted based on body weight. Doses and routes were informed by previous studies demonstrating the analgesic and neuroprotective effects of vinpocetine in preclinical models of pain and central nervous system disorders [32,36]. For intrathecal injection, vinpocetine was prepared as a 1.43 mM solution and 10 μl was injected per mouse (0.2 mg/kg). Mice were anesthetized with isoflurane (Hana Pharm, Songnam, Gyeonggi, South Korea), and the hair on their back was gently shaved to facilitate identification of the lumbar 5 (L5) level. The drug was then slowly injected into the spinal cavity using a 31-gauge needle attached to a 50 μl Hamilton syringe. After administration, the needle was held in place for 1 min before withdrawal to prevent reflux.

To assess the analgesic effect of vinpocetine in oxidative stress-induced pain models, pain was induced using Antimycin A (A8674, Sigma-Aldrich) and potassium superoxide (355420250, Thermo Scientific Chemicals, Waltham, MA, USA). Antimycin A (A.A) was dissolved in DMSO and diluted in 1 × phosphate-buffered saline (PBS) to a final concentration of 50 μM. A volume of 10 μl was injected intrathecally (i.t.) [37]. The control group received an equivalent volume of DMSO diluted in 1 × PBS to match the experimental conditions. KO_2 was prepared at a concentration of 100 mM in PBS and 5 μl was administered (i.t.).

All injections were performed under strict aseptic conditions, and the mice were monitored post-injection for signs of distress or adverse reactions.

2.4. Behavioral assessment

Mice were randomly assigned to the treatment groups. Behavioral testing was performed in a blinded manner, with the experimenters unaware of the treatment allocations.

Mechanical hypersensitivity was assessed using the up-down method with a series of von Frey filaments (Stoelting, Chicago, IL, USA) as described in our previous study [38]. Each filament was applied to the plantar surface of the hindpaw until it bent slightly, and paw withdrawal, shaking, or flinching were considered positive responses. The 50 % mechanical withdrawal threshold (MWT) was calculated.

Thermal hypersensitivity was measured using the Hargreaves test with a plantar test device (7371 plantar test; UgoBasile, Milano, Italy). Mice were allowed to acclimate within an open-topped transparent plastic cylinder (6 cm diameter × 16 cm height) on a glass floor for 20 min before the test. A mobile radiant heat source was then placed under the glass floor and focused on the hindpaw. The infrared (IR) intensity was set at 50 %, which is considered optimal for preventing tissue damage while eliciting paw withdrawal latency (PWL). PWLs were measured with a cut-off time of 20 s. Heat stimulation was repeated five times with a 10-minute interval to obtain the mean latency of paw withdrawal.

Cold hypersensitivity was assessed by observing foot withdrawal responses (lifting, shaking, or licking) following the application of cold stimuli to the plantar surface of the paw. A drop of 100 % acetone was applied delicately to the left hind paw of each mouse using a 1 cc syringe connected to a PE10 tube. The test was repeated five times, with an interval of approximately 3–5 min between each repetition. The response frequency to acetone was expressed as a percentage of the response frequency.

2.5. in vivo detection of mitochondrial ROS

MitoSOX Red (M36008, Invitrogen, Carlsbad, CA, USA) was dissolved in DMSO to create a 5 mM stock solution and then diluted with 0.9 % sterile saline to a final concentration of 33 μM. On PID14, the mice were anesthetized with isoflurane anesthesia, and 10 μl of MitoSOX Red was injected (i.t.). Approximately 5–6 h (vinpocetine was administered 2 h before MitoSOX Red injection) after MitoSOX Red injection, the mice were euthanized, and the L4-L6 spinal cord segments were removed and post-fixed in 4 % paraformaldehyde (PFA) overnight at 4°C. The spinal cord was then equilibrated in 30 % sucrose solution for 2 days. Tissues were embedded in an Optimal Cutting Temperature compound (O.C.T.; Sakura Finetek, Torrance, CA, USA) and cryosectioned at 20 μm thickness, then mounted on gelatin-coated slides. The sections were washed with 1 × PBS for 10 min, three times, and coverslipped with mounting medium (H-1000, Vector Laboratories, Burlingame, CA, USA). The sections were examined under a fluorescence microscope with a rhodamine filter. Laminae III-V of the dorsal horn were photographed from 2 randomly selected sections from each animal. Images were captured using an LSM710 microscope (Carl Zeiss, Jena, Germany) with a 63 × oil objective lens and were saved as digital image files. The intensity of MitoSOX Red-positive puncta, identified by their localization around the nuclei (dark, oval-shaped areas), was quantified from these images.

2.6. Western blot analysis

On PID14, after the last injection of vinpocetine, L4-L6 spinal cord segments were collected and immediately frozen in liquid nitrogen, and stored at −70℃ until analysis. The tissues were homogenized with a mixture of lysis buffer (PRO-PREP; Intron Biotechnology, Pyeongtaek, South Korea) and protease inhibitor cocktail (P8340; Sigma-Aldrich) and centrifuged at 15,000 rpm for 10 min. The supernatants containing proteins were transferred into a clean tube. The Protein concentration was measured using a BCA kit. Twenty micrograms (20 μg) of total protein were prepared and loaded onto an 8 %-10 % acrylamide gel, followed by PVDF membrane transfer (Merck Millipore, Darmstadt, Germany). The membranes were blocked with 5 % skim milk (SM2010; GeorgiaChem, Norcross, GA, USA) for 1 h at RT, and then were incubated with the primary antibody overnight at 4℃. The primary antibodies used were PGC-1α (1:1000, PA5–72948, Thermo Fisher Scientific, Waltham, MA, USA), NRF-1 (1:1000, no. 46743, Cell Signaling Technology, Beverly, MA, USA), TFAM (1:3000, NBP2–19437, Novusbio, CO, USA), anti-SOD2 (1:5000, ab13533, Abcam, Cambridge, UK), AMPA (1:5000, ab183797, Abcam), NR2A (1:1000, ab124913, Abcam), NR2B (1:2500, ab65783, Abcam), PKC-α (1:5000, ab11723, Abcam), CaMKII-α (1:5000, ab52476, Abcam), and PKA (1:5000, ab75991, Abcam). GAPDH (1:10000, LF-PA0018, ABFrontier, Seoul, South Korea) was used as an internal loading control. All antibodies used were commercially validated and have been widely used. The membrane was then incubated with a secondary anti-rabbit antibody (1:5000; no. 7074, CST) for 2 h at RT. The antibody-labeled protein bands were imaged using an enhanced chemiluminescence reagent (ECL; RPN2232, Cytiva, Marlborough, MA, USA). The bands were detected using the Cytiva system (IQ800) and the intensities were quantified using ImageJ.

2.7. Immunohistochemistry

On PID14, after the last vinpocetine treatment, the animals were deeply anesthetized with sodium pentobarbital (50 mg/kg, i.p.) and perfused transcardially with 0.9 % sterile saline followed by 4 % PFA (pH 7.4). The L4-L5 spinal cords were isolated, and post-fixed in 4 % PFA overnight at 4°C and cryoprotected in 30 % sucrose in PBS until sinking. Tissues were embedded in O.C.T., rapidly frozen in liquid nitrogen, and stored at −70°C. Transverse cryosections (20 μm thick) were mounted onto glass slides for immunofluorescence staining. For antigen retrieval, sections were incubated in 10 mM sodium citrate buffer (pH 6.0) at 95°C for 10 min, washed with PBS, and permeabilized with 0.3 % PBST (PBS + 0.3 % Triton X-100). After blocking with 10 % normal donkey serum in 0.3 % PBST for 1 h at room temperature (RT), sections were incubated overnight at 4°C with the following primary antibodies: anti-glutamate receptor 1 (GluR1, AMPA subtype; EPR19522, 1:200, ab183797, Abcam), NeuN (1:1000, ab104222, Abcam), and PKC-α (1:500, A302–446A, Thermo Fisher Scientific). After washing with PBS, the sections were incubated with fluorescently labeled secondary antibodies for 2 h at RT in the dark, followed by DAPI (4′,6-diamidino-2-phenylindole) (H-1200, Vector Laboratories) nuclear counterstaining. The slides were cover-slipped and sealed. Fluorescent images were captured using a Zeiss LSM 700 laser scanning confocal microscope (Carl Zeiss) at 20 × and 40 × magnifications. For each animal, 3 sections were selected, and 2–3 non-overlapping regions of interest (ROI) were imaged per section from the dorsal horn. Maximum intensity projection (MIP) was generated using Zen Black software (Carl Zeiss). Quantitative analysis of fluorescence intensity, including stained area and mean fluorescence intensity (MFI), was performed using ImageJ (NIH, Bethesda, MD, USA). For intensity quantification, grayscale thresholding was applied using a fixed range of 56–255 and binary images were generated to define ROIs. The fluorescence intensity values were normalized prior to statistical analysis. Colocalization analysis was conducted using the colocalization module in the Zen Blue software (Carl Zeiss). From each ROI, the software automatically calculated the colocalized area, Pearson's correlation coefficient, and Mander's overlap coefficients based on channel overlap. The same acquisition and processing parameters were used for all the experimental groups.

2.8. Voltage-sensitive dye imaging (VSDI)

On PID14 (Fig. S1A), the mice were deeply anesthetized with urethane (1.25 g/kg, i.p.) and transcardially perfused with ice-cold solution containing 213 mM sucrose, 2.5 mM KCl, 1.25 mM NaH_2PO_4, 10 mM $MgSO_4$, 0.5 mM $CaCl_2$, 26 mM $NaHCO_3$, and 11 mM glucose. The spinal cord, including L4-L5, was carefully removed and rapidly cooled in ice-cold solution for 5 min. The spinal cord was mounted on an agarose block and sectioned into 400-μm thick transverse slices using a vibratome (Leica Biosystems Inc., Buffalo Grove, IL, USA). Sections were incubated in oxygenated artificial cerebrospinal fluid (aCSF) for 1 h at RT before staining with voltage-sensitive dye (VSD; di-2-ANEPEQ, 50 μg/mL in saline). The sections were immediately transferred to interface chambers filled with oxygenated artificial cerebrospinal fluid (aCSF; 126 mM NaCl, 2.5 mM KCl, 1.25 mM NaH_2PO_4, 2 mM $MgCl_2$, 2 mM $CaCl_2$, 26 mM $NaHCO_3$, and 10 mM glucose, saturated with 95 % O_2 and 5 % CO_2 (pH 7.2)). Following 1 h of recovery at RT in flowing aCSF, the sections were stained for 1 h with voltage-sensitive dye (VSD; di-2-ANEPEQ, 50 μg/mL in saline; Molecular Probes, Eugene, OR, USA).

For optical imaging, a concentric bipolar microelectrode (30213, FHC, Bowdoin, ME, USA) was carefully placed in the region of interest (ROI) under an optical microscope (Olympus Optical Co. Ltd., Tokyo, Japan) equipped with a 10 × objective and a 0.35 × projection lens, positioned above the recording site. Electrical stimulation was delivered as square pulses (width: 2 ms, inter-stimulus interval: 5 s, intensity adjusted to evoke responses) using a stimulus-isolation unit (World Precision Instruments, Sarasota, FL, USA). Neuronal signals were

recorded using a high-resolution CCD camera (Brainvision Inc., Tokyo, Japan) equipped with a dichroic mirror, an excitation filter (510–555 nm), and an absorption filter (590 nm). A 150 W tungsten-halogen lamp served as the fluorescence source. The imaging area comprised 184 × 124 pixels.

The change in fluorescence intensity was recorded for 943.5 ms per trial, averaged over 20 trials. Optical signals were acquired using an optical imaging recording system (MiCAM02, Brainvision Inc.) at a frame rate of 3.7 ms/frame. To normalize the fluorescence intensity across pixels, the intensity change (ΔF) in each pixel was expressed as a fractional change relative to the initial fluorescence intensity (F), ΔF/F. The amplitudes of the optical signals and the size of the activated areas were determined using a spatial filter (9 × 9 pixels) and a cubic filter (3 × 3 pixels). Data collection and analysis were performed using BV Analyzer software (Brainvision Inc.). Optical signals were quantified as %ΔF/F, representing the fractional fluorescence change within a region of interest (ROI) with a radius of 2, specifically in the dorsal horn of the spinal cord. Changes in the optical intensity and activation area changes were systematically analyzed.

2.9. Statistical analysis

Power analysis was performed using G*Power 3.1, assuming a medium effect size (f = 0.25 for ANOVA, corresponding to Cohen's $d = 0.5$ for *t*-tests), a significance level (α) of 0.05, and a statistical power (1 − β) of 0.80. Statistical analyses were performed using GraphPad Prism 10.1.0 (GraphPad Software, San Diego, CA, USA). Behavioral test data for the von Frey filament test, Hargreaves test, and acetone test were analyzed using two-way ANOVA with Bonferroni's post hoc test. Western blot and immunohistochemistry data were analyzed using one-way ANOVA followed by Tukey's post hoc test. Differences in optical signal intensities and activated areas were analyzed using paired *t*-test and two-way ANOVA, followed by Bonferroni's post hoc test. All values are presented as means ± standard error of the mean (SEM). P values less than 0.05 were considered to indicated statistically significant.

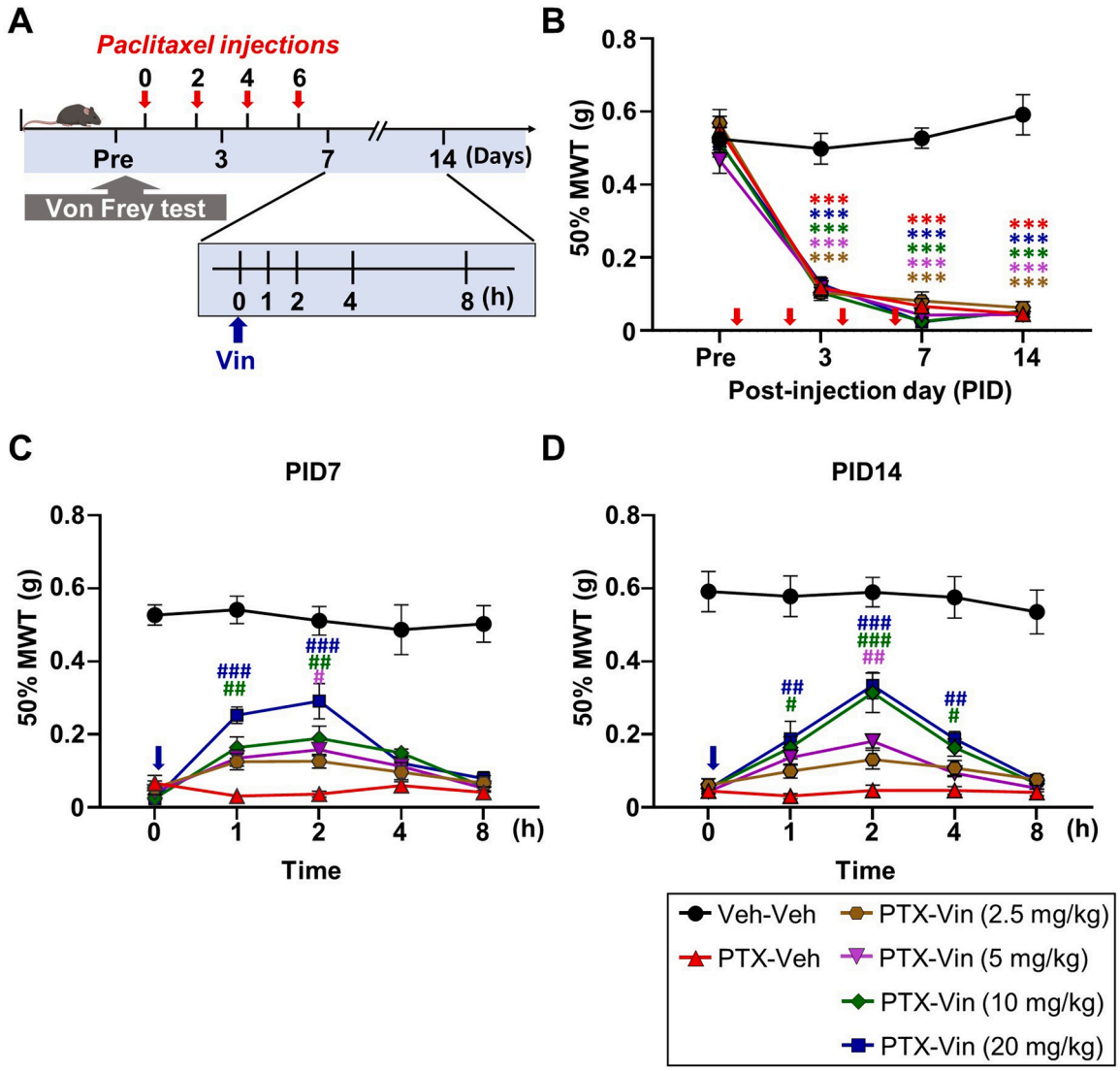

Fig. 1. Evaluation of mechanical hypersensitivity in the CIPN model following single vinpocetine administration. (A) Schematic representation of the experimental timeline for drug administration and behavioral tests. Blue arrows indicate vinpocetine (Vin) or vehicle (Veh) treatment. (B) Progression of mechanical hypersensitivity following intraperitoneal paclitaxel injection (n = 7 per group). $^{***}P < 0.001$ vs. Veh-Veh group, as determined using two-way ANOVA with repeated measures followed by Bonferroni's post hoc multiple comparison test. (C, D) Analgesic effects of a single intraperitoneal vinpocetine treatment on mechanical hypersensitivity (n = 7 per group), as indicated by the 50 % mechanical withdrawal threshold (MWT) on PID7 (C) and PID14 (D). $^{\#}P < 0.05$, $^{\#\#}p < 0.01$, and $^{\#\#\#}p < 0.001$ vs. PTX-Veh group, as determined using two-way ANOVA with repeated measures followed by Bonferroni's post hoc multiple comparison test.

3. Results

3.1. Acute vinpocetine administration alleviates mechanical hypersensitivity

To evaluate the antinociceptive effect of vinpocetine in CIPN, we tested four dosages (2.5, 5, 10, and 20 mg/kg) using the von Frey filament test on PID7 and PID14. The mice received paclitaxel (PTX, 2 mg/kg, i.p.) every other day for a total of four injections (PID0, 2, 4, and 6). The von Frey test was performed on PID3, PID7, and PID14 (Fig. 1A). PTX-treated mice exhibited a significant reduction in 50 % MWT by PID3, which persisted through PID14, confirming the successful establishment of the CIPN model (Fig. 1B; Pre: $p < 0.001$; PID3: $p < 0.001$; PID7: $p < 0.001$; PID14: $p < 0.001$ for days: $F_{3,\ 108} = 417.0$, $p < 0.001$; for groups: $F_{5,\ 36} = 62.53$, $p < 0.001$; for days × groups: $F_{15,\ 108} = 19.79$).

On PID7, vinpocetine was administered i.p. after the pre-test (0 h), and 50 % MWTs were assessed at 1, 2, 4, and 8 h post-administration. At the 1-hour timepoint, mice receiving 10 or 20 mg/kg vinpocetine (PTX-Vin) exhibited significantly higher 50 % MWTs compared to the vehicle-treated (PTX-Veh) group (10 mg/kg: $p = 0.0096$; 20 mg/kg: $p < 0.001$; for time: $F_{5,\ 180} = 19.82$, $p < 0.001$; for groups: $F_{5,\ 36} = 101.2$, $p < 0.001$; for time × groups: $F_{25,\ 180} = 5.029$, $p < 0.001$). By 2 h, the 50 % MWTs remained significantly elevated in the 5, 10, and 20 mg/kg groups, with the 20 mg/kg dose demonstrating the greatest effect (5 mg/kg: $p = 0.026$; 10 mg/kg: $p = 0.0014$; 20 mg/kg: $p < 0.001$). However, by 4 h, no significant differences were observed between vinpocetine-treated groups and the PTX-Veh groups (Fig. 1C). To further confirm the analgesic effect of vinpocetine during the fully developed phase of CIPN, additional dose-response experiments were performed on PID14 (Fig. 1D). A similar trend was observed, with 10 and 20 mg/kg vinpocetine significantly increasing 50 % MWTs at 1, 2, and 4 h post-

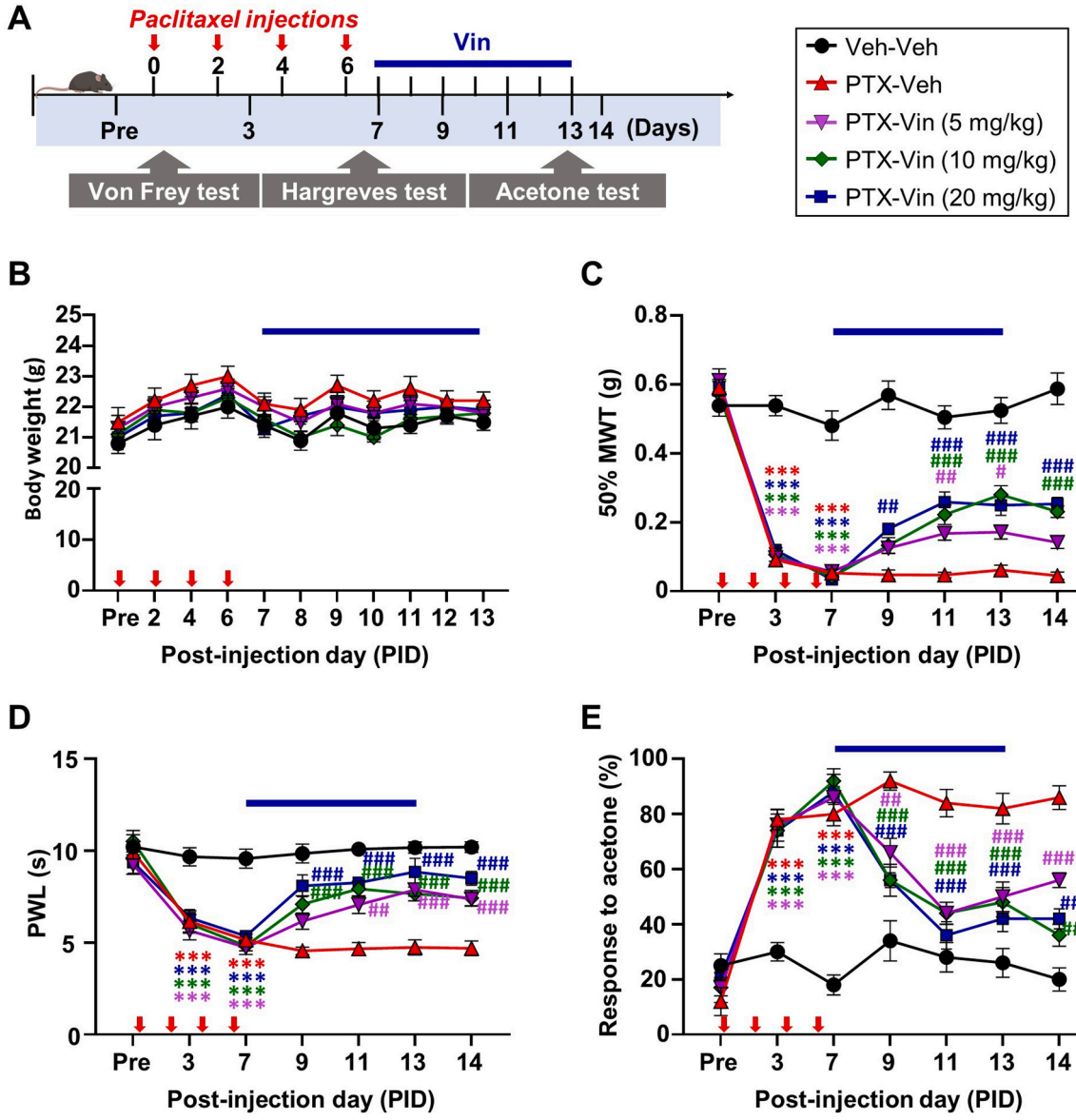

Fig. 2. Effects of repetitive vinpocetine administration from PID7 to PID13 in the CIPN model. (A) Experimental timeline depicting vinpocetine treatment and behavioral assessments. Blue bars represent intraperitoneal vinpocetine (Vin) or vehicle (Veh) treatment from PID7 to PID13 following behavioral tests. (B) Changes in body weight over time (n = 10 per group). (C-E) Analgesic effects of Vin were evaluated by assessing mechanical hypersensitivity (n = 10 per group) using 50 % MWT (C), thermal sensitivity via paw withdrawal latency (PWL) (D), and cold hypersensitivity indicated by the percentage response to acetone (E). $^{**}p < 0.001$ vs. Veh-Veh group, $^{\#}p < 0.05$, $^{\#\#}p < 0.01$, and $^{\#\#\#}p < 0.001$ vs. PTX-Veh group, as determined using two-way ANOVA with repeated measures followed by Bonferroni's post hoc multiple comparison test.

administration, peaking at 2 h (10 mg/kg, 1 h: $p = 0.0339$, 2 h: $p < 0.001$; 20 mg/kg, 1 h: $p = 0.0049$, 2 h: $p < 0.001$; 4 h: $p = 0.0176$; for time: $F_{5,\ 180} = 31.64$, $p < 0.001$; for groups: $F_{5,\ 36} = 85.03$, $p < 0.001$; for time × groups: $F_{25,\ 180} = 2.584$, $p < 0.001$). The 10 mg/kg and 20 mg/kg doses produced comparable peak effects, and by 8 h, 50 % MWTs in the vinpocetine-treated groups were indistinguishable from those in the PTX-Veh group (Fig. 1D). These results indicate that vinpocetine provides transient yet significant analgesia in CIPN, with 20 mg/kg exhibiting the most pronounced effect within 1–2 h post-administration. These results support the potential use of vinpocetine as a therapeutic agent for CIPN.

3.2. Repeated vinpocetine administration alleviates mechanical, thermal, and cold hypersensitivity in a CIPN model

Based on prior experiments validating the antinociceptive effects of vinpocetine at doses of 5, 10, and 20 mg/kg, these doses were selected for further evaluation. Vinpocetine was administered i.p. once daily from PID7 to PID13 in the CIPN model to assess its cumulative analgesic effects. Behavioral tests were conducted on PID9, PID11, PID13, and PID14 (Fig. 2A). Body weight measurements taken before drug administration showed no significant differences among the groups (Fig. 2B).

Following the development of pain on PID7 in the von Frey filament test, the 50 % MWTs in the PTX-Veh and PTX-Vin groups were significantly higher than those in the Veh-Veh group (Fig. 2C). On PID9, 50 % MWTs were significantly increased in the 20 mg/kg group compared to the PTX-Veh group ($p = 0.002$). For PID11 and PID13, all PTX-Vin groups (5, 10, and 20 mg/kg) showed significant improvement, with 10 mg/kg and 20 mg/kg doses demonstrating similar efficacy (5 mg/kg, PID11: $p = 0.0071$, PID13: $p = 0.0204$; 10 mg/kg, PID11: $p < 0.001$, PID13: $p < 0.001$; 20 mg/kg, PID11: $p < 0.001$, PID13: $p < 0.001$). On PID14, 50 % MWTs remained stable, indicating sustained analgesic effects (10 mg/kg and 20 mg/kg, $p < 0.001$).

In the Hargreaves test, paw withdrawal latency (PWL, in seconds) was measured to assess thermal hypersensitivity, which was evident in the PTX-treated groups on PID3 and PID7 (Fig. 2D, $p < 0.001$; for days: $F_{6,\ 270} = 40.75$, $p < 0.001$; for groups: $F_{4,\ 45} = 55.53$, $p < 0.001$; for days × groups: $F_{24,\ 270} = 5.464$). On PID9, PWLs were significantly higher in the PTX-Vin groups than in the PTX-Veh group (10 and 20 mg, $p < 0.001$). This trend continued on PID11 and PID13, with 20 mg/kg groups showing greater improvements than the 5 mg/kg and 10 mg/kg groups (5 mg/kg, PID11: $p = 0.0017$, PID13, $p < 0.001$; 10 mg/kg, PID11: $p < 0.001$, PID13: $p < 0.001$; 20 mg/kg, PID11: $p < 0.001$, PID13: $p < 0.001$). Significant differences persisted across all PTX-Vin groups on PID14 compared to the PTX-Veh group (5, 10, 20 mg/kg, $p < 0.001$).

The acetone test was used to evaluate cold hypersensitivity in the CIPN model. Responses to acetone (as a percentage) were measured before PTX injection (Pre), and on PID3 and PID7. The results showed that PTX-treated mice exhibited increased cold sensitivity to PID7 (Fig. 2E; PID3 and PID7: $p < 0.001$; for days: $F_{6,\ 270} = 79.04$, $p < 0.001$; for groups: $F_{4,\ 45} = 45.96$, $p < 0.001$; for days × groups: $F_{24,\ 270} = 10.92$). On PID9, all PTX-Vin groups showed a marked reduction in responses compared to the PTX-Veh group (5 mg/kg, $p = 0.017$; 10 and 20 mg/kg, $p < 0.001$). This decline persisted on PID11 and PID13 across all doses (5, 10, 20 mg/kg, PID11 and PID13, $p < 0.001$). Although a slight increase was observed on PID14, the responses remained significantly lower than those in the PTX-Veh group ($p < 0.001$).

Overall, repeated vinpocetine administration at 5, 10, and 20 mg/kg effectively alleviated mechanical, thermal, and cold hypersensitivity in a dose-dependent manner, with 10 and 20 mg/kg providing superior and sustained analgesic effects.

3.3. Intrathecal vinpocetine relieves CIPN-induced mechanical hypersensitivity

To determine whether vinpocetine exerts its analgesic effects at the spinal level in the CIPN model, this experiment evaluated its efficacy and site of action. Following full CIPN establishment, vinpocetine was administered i.t. on PID7 and PID14 at a concentration of 1.43 mM in 10 μl, based on the effective intraperitoneal dose of 20 mg/kg (Fig. 3A). Baseline von Frey filament test was conducted before vinpocetine administration, and 50 % MWTs were measured at 1, 2, 4, and 8 h post-treatment. On PID7, intrathecal vinpocetine administration significantly increased 50 % MWTs compared to the PTX-Veh group, with effects emerging at 1 and 2 h post-treatment and persisting up to 4 h (Fig. 3B; 1 h: $p = 0.0031$; 2 h: $p < 0.001$; for time: $F_{4,\ 60} = 5.080$, $p < 0.01$; for groups: $F_{2,\ 15} = 175.6$, $p < 0.001$; for time × groups: $F_{8,\ 60} = 3.854$, $p < 0.001$). By 8 h, 50 % MWTs returned to levels comparable to those in the PTX-Veh group. The results observed on PID14 were consistent with those on PID7, showing that the antinociceptive effect of vinpocetine was evident at 1 h, peaked at 2 h, and remained significant until 4 h before returning to baseline (Fig. 3C; 1 h: $p = 0.0048$, 2 h: $p < 0.001$; for time: $F_{4,\ 60} = 3.569$, $p < 0.05$; for groups: $F_{2,\ 15} = 142.0$, $p < 0.001$; for time × groups: $F_{8,\ 60} = 3.869$, $p < 0.001$). These findings confirm that intrathecal vinpocetine alleviates CIPN-induced mechanical hypersensitivity, supporting its action at the spinal cord level.

3.4. Repeated vinpocetine treatment mitigates oxidative stress and restores mitochondrial biogenesis

To investigate the mechanisms underlying the analgesic effect of vinpocetine in CIPN, MitoSOX Red staining and Western blot analyses were performed following repeated intraperitoneal vinpocetine treatment. MitoSOX Red staining was used to assess mitochondrial ROS levels in the spinal cord dorsal horn, specifically in Lamina III-V. Oxidized MitoSOX labeling appeared as fluorescent granules in the cytoplasmic region (Fig. 4A). The density of red granules varied among the experimental groups, prompting quantification of the fluorescence intensity. The results revealed a significant increase in fluorescence intensity in the PTX-Veh group compared to the Veh-Veh group, indicating elevated levels of mitochondrial ROS (Fig. 4B, $p < 0.001$; $F_{2,\ 21} = 14.45$, $p < 0.001$). Vinpocetine treatment reduced this intensity, suggesting attenuation of oxidative stress ($p = 0.0222$). Western blot analysis showed that SOD2 expression was downregulated in the PTX-Veh group compared with that in the Veh-Veh group (Fig. 4C, $p = 0.0013$; $F_{2,\ 18} = 12.54$, $p = 0.0004$). However, vinpocetine treatment restored SOD2 levels ($p = 0.0011$), further supporting its role in reducing oxidative stress.

To assess the effect of vinpocetine on mitochondrial biogenesis in the spinal cord, Western blot analysis was performed for key regulators, including PGC-1α, NRF1, and TFAM. PGC-1α, a master regulator of mitochondrial biogenesis [39], was significantly reduced in the PTX-Veh group ($p = 0.0348$; $F_{2,\ 15} = 5.451$, $p = 0.0124$) but was upregulated following vinpocetine treatment (Fig. 4D, $p = 0.018$). Similarly, NRF1, a downstream mediator of PGC-1α [40], was downregulated in the PTX-Veh group ($p = 0.0071$; $F_{2,\ 18} = 6.645$, $p = 0.0069$), but significantly increased in the PTX-Vin group (Fig. 4E, $p = 0.0399$). TFAM expression, which was suppressed in the PTX-Veh group ($p < 0.001$; $F_{2,\ 15} = 16.66$, $p = 0.0002$), was also restored by vinpocetine treatment (Fig. 4F, $p = 0.0033$).

To further investigate the role of vinpocetine in oxidative stress-related pain, its effects were examined in A.A- and KO_2-induced pain models. Intrathecal A.A administration induced significant mechanical hypersensitivity 8 h post-injection, indicating the establishment of pain ($p < 0.001$; for time: $F_{5,\ 75} = 48.70$, $p < 0.001$; for groups: $F_{2,\ 15} = 43.33$, $p < 0.001$; for time × groups: $F_{10,\ 75} = 12.23$, $p < 0.001$). At this time point, intrathecal vinpocetine administration significantly increased the 50 % MWT within 1 h ($p = 0.019$), peaking at 2 h

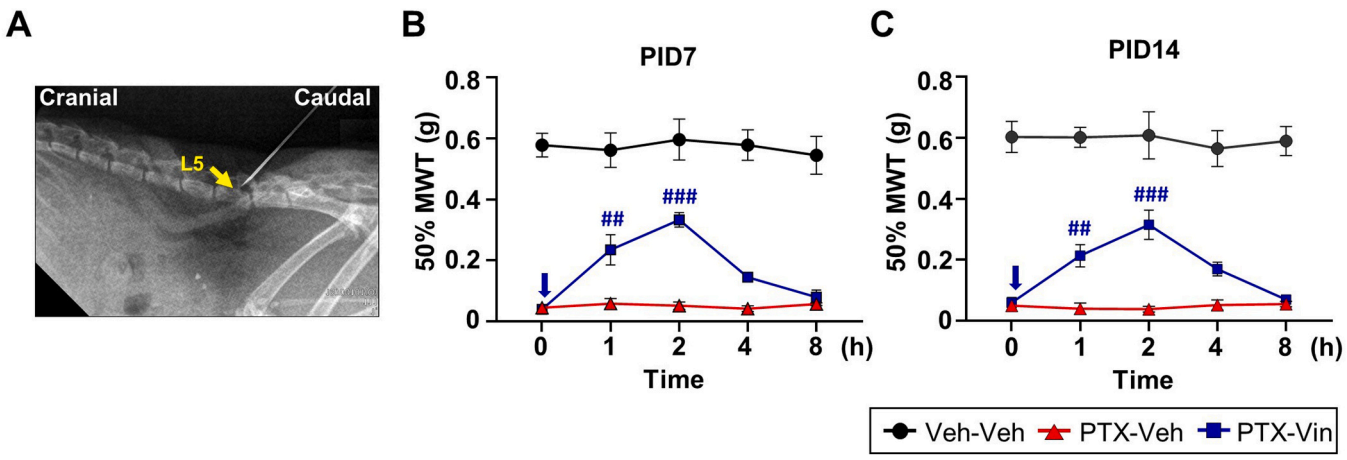

Fig. 3. Analgesic effect of a single intrathecal vinpocetine administration in the CIPN model. (A) X-ray confirmation of the intrathecal injection site, with the yellow arrow indicating the lumbar 5 (L5) spine. (B, C) Analgesic effect of intrathecal vinpocetine (n = 6 per group) assessed by 50 % MWT on PID7 (B) and PID14 (C). Blue arrows indicate vinpocetine (Vin) or vehicle (Veh) treatment. $^{\#\#}P < 0.01$, $^{\#\#\#}p < 0.001$ vs. PTX-Veh group, as determined using two-way ANOVA with repeated measures followed by Bonferroni's post hoc multiple comparison test.

($p < 0.001$), demonstrating its analgesic efficacy in A.A-induced pain (Fig. 4G). In the KO_2 model, to determine whether the antinociceptive effects of vinpocetine are mediated through superoxide anion scavenging, it was administered 1 h before KO_2 injection. The KO_2-Veh group exhibited significant mechanical hypersensitivity post-injection ($p < 0.001$, KO_2-Veh group vs. Veh-Veh group; for time: $F_{6,\ 90} = 5.985$, $p < 0.001$; for groups: $F_{2,\ 15} = 5.034$, $p = 0.0212$; for time × groups: $F_{12,\ 90} = 2.914$, $p = 0.0019$), while vinpocetine treatment mitigated pain at 0.5 ($p < 0.001$) and 1 h (Fig. 4H, $p = 0.0168$). By 1.5 h, the pain resolved spontaneously, with no differences observed at 2 and 4 h. These results suggest that vinpocetine scavenges ROS, thereby reducing oxidative stress and pain sensitization at the spinal level.

Taken together, these results indicate that vinpocetine alleviates CIPN by reducing oxidative stress and promoting mitochondrial biogenesis in the spinal cord. Its effects on mitochondrial ROS, SOD2, and PGC-1α/NRF1/TFAM pathway highlight its role in oxidative stress modulation. Its efficacy in A.A- and KO_2-induced pain models further supports its potential as an ROS-targeting analgesic for neuropathic pain.

3.5. Vinpocetine treatment reduces neuronal activity in the spinal cord dorsal horn of the CIPN model

To investigate the effect of CIPN on neuronal excitability, VSDI was performed on spinal cord slices on PID14 in the CIPN model. As an initial step, the minimal electrical stimulation intensity required to evoke detectable neuronal responses was determined. The electrical stimulation was incrementally increased from 0.1 mA. As shown in Fig. 5A, neuronal signals became progressively stronger and more widespread with increasing stimulation intensity. Notably, the differences between the Veh and PTX groups became apparent at 0.3 mA ($p = 0.0137$), identifying it as the threshold for detecting hyperexcitability (Fig. 5B). While peak amplitudes in the PTX group increased at 0.4 and 0.5 mA compared to the Veh group, the differences were not statistically significant. However, at 1 mA, the PTX group exhibited significantly greater peak amplitudes ($p = 0.0307$), confirming neuronal hypersensitivity in CIPN. These results suggest that neuronal hyperexcitability under CIPN conditions becomes detectable at 0.3 mA, making it a reliable marker for further investigation.

Since 0.3 mA was identified as the threshold, 0.3, 0,6 and 1.2 mA were selected to assess the effects of vinpocetine in the CIPN model. DMSO served as the control, and each stimulation intensity was tested in three phases: before vinpocetine or DMSO treatment (Pre), immediately after vinpocetine or DMSO treatment (Treat.), and after the treatment (Post) (Fig. S1B). Representative optical images of the spinal cord in the CIPN model, comparing the DMSO- and vinpocetine-treated groups, are shown in Fig. 5C. These images illustrate decreased neuronal signals during the vinpocetine treatment phase at 0.6 and 1.2 mA. Vinpocetine or DMSO was applied for 15 min before recording responses. To evaluate neuronal activity over time, the fluorescence responses across time points for each stimulation intensity were plotted (Fig. 5D). These traces represent changes in peak amplitude (% ΔF/F) over time, with the treatment phase highlighted using shaded colors to distinguish it from the pre- and post-phases. Based on these time-series data, the area under the curve (AUC) was calculated for each phase as a measure of cumulative neuronal activity (Fig. 5E). At 0.3 and 0.6 mA, the AUC values remained comparable between the DMSO and Vin groups across all the phases. However, at 1.2 mA stimulation, the Vin group exhibited a marked reduction in AUC compared to the DMSO group ($p = 0.0304$; for phases: $F_{2,\ 32} = 4.775$, $p = 0.0153$; for groups: $F_{1,\ 16} = 1.125$, $p > 0.05$; for phases × groups: $F_{2,\ 32} = 5.765$, $p = 0.0073$). Separately, to assess the magnitude of neuronal responses, peak amplitude values were analyzed specifically within the 200–400 ms window after stimulation (Fig. 5F). While the Vin group showed a slight decline in peak amplitude at 0.3 and 0.6 mA, only the 1.2 mA condition revealed a significant reduction during the treatment phase ($p = 0.0493$; For phases: $F_{2,\ 32} = 6.536$, $p = 0.0042$; for groups: $F_{1,\ 16} = 0.7808$, $p > 0.05$; for phases × groups: $F_{2,\ 32} = 6.697$, $p = 0.0037$).

Taken together, these results indicate that vinpocetine reduces neuronal hyperexcitability in a stimulation-dependent manner. This effect was particularly pronounced at higher stimulation intensities, particularly at 1.2 mA.

3.6. Repeated vinpocetine treatment inhibited AMPA and NR2B expression in the spinal cord of a CIPN model

To investigate the role of AMPA, NR2A, and NR2B receptors in CIPN-induced spinal plasticity and their modulation by vinpocetine, Western blot analysis was performed on PID14 following repetitive vinpocetine treatment (i.p.). Western blot results showed that AMPA receptor expression was significantly upregulated in the PTX-Veh group compared to the Veh-Veh group (Fig. 6A, $p = 0.0033$; $F_{2,\ 15} = 8.770$, $p = 0.003$), suggesting enhanced excitatory synaptic transmission in CIPN. However, vinpocetine treatment significantly reduced AMPA receptor expression in the PTX-Vin group ($p = 0.0182$), indicating its role in suppressing CIPN-induced excitatory synaptic potentiation and restoring synaptic homeostasis. In contrast, NR2A receptor expression remained unchanged between the PTX-Veh and PTX-Vin groups

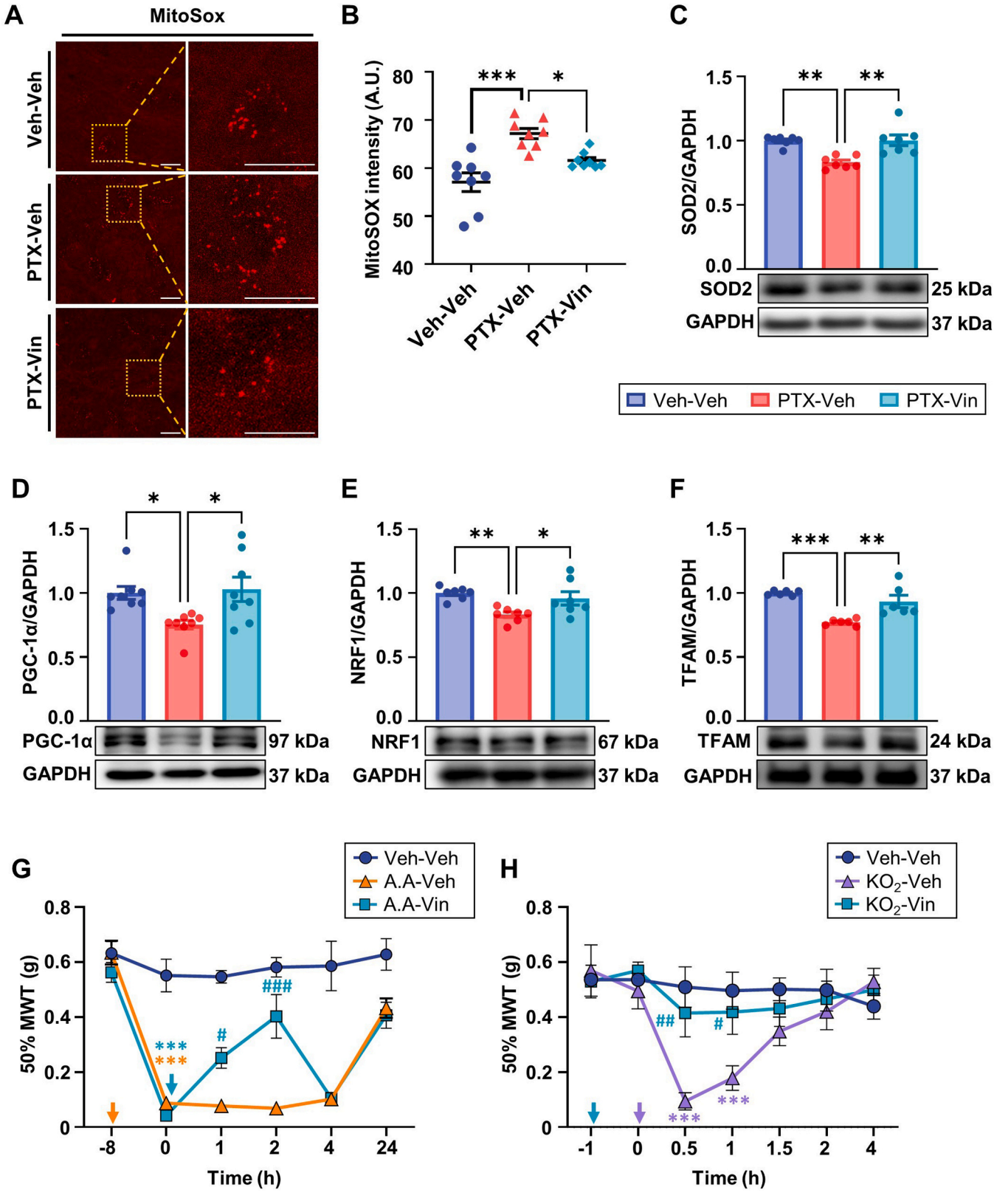

(caption on next page)

Fig. 4. Effect of vinpocetine on mitochondrial ROS, biogenesis, and oxidative stress-induced pain models. (A) Representative fluorescence images of spinal cord sections labeled with MitoSOX Red to detect mitochondrial ROS levels. Scale bar = 20 μm. (B) Quantification of MitoSOX Red intensity in the spinal cord among the groups after repetitive intraperitoneal vinpocetine treatment (n = 8 per group). *P < 0.05, ***p < 0.001, as determined using one-way ANOVA followed by Tukey's post hoc multiple comparison test. (C-F) Western blot analysis of the expression levels of SOD2 (C, n = 7 per group), PGC-1α (D, n = 8 per group), NRF1 (E, n = 7 per group), and TFAM (F, n = 7 per group). *P < 0.05, **p < 0.01, ***p < 0.001, as determined using one-way ANOVA followed by Tukey's post hoc multiple comparison test. The original Western blot bands are shown in Fig. S2. (G) Pain-relieving effect of intrathecal vinpocetine in an antimycin A (A.A)-induced pain model. A.A was given intrathecally. The 50 % MWT was measured using von Frey filaments (n = 6 per group). The orange arrow indicates A.A administration, and the light blue arrows indicate vinpocetine (Vin) or vehicle (Veh) treatment. ***P < 0.001 vs. Veh-Veh group, #p < 0.05, ###p < 0.001 vs. A.A-Veh group, as determined using two-way ANOVA with repeated measures followed by Bonferroni's post hoc multiple comparison test. (H) Analgesic effect of vinpocetine in a potassium superoxide (KO_2)-induced pain model measured using von Frey filaments. KO_2 was administered intrathecally (n = 6 per group). The purple arrow indicates KO_2 administration, and the light blue arrow indicates Vin or vehicle Veh treatment. ***P < 0.001 vs. Veh-Veh group, #p < 0.05, ##p < 0.01 vs. KO_2-Veh group, as determined using two-way ANOVA with repeated measures followed by Bonferroni's post hoc multiple comparison test.

(Fig. 6B), suggesting that NR2A-containing NMDA receptors are not the primary mediators of CIPN-induced plasticity. Meanwhile, NR2B receptor expression was significantly elevated in the PTX-Veh group ($p = 0.009$; $F_{2,\ 15} = 8.603$, $p = 0.0032$) and reduced by vinpocetine treatment (Fig. 6C, $p = 0.0057$), indicating that vinpocetine attenuates NR2B-mediated excitatory neurotransmission and pain sensitization.

IHC staining further confirmed increased AMPA receptor expression in the superficial dorsal horn of the PTX-Veh group (Fig. 6D). Mean fluorescence intensity analysis revealed that AMPA receptor expression was significantly higher in the PTX-Veh group than in the Veh-Veh group (Fig. 6E, $p < 0.001$; For groups, $F_{2,\ 105} = 42.82$, $p < 0.001$). Similarly, AMPA receptor expression was significantly reduced in the PTX-Vin group compared with that in the PTX-Veh group ($p < 0.001$). Colocalization analysis with NeuN, a neuronal marker, revealed an increased colocalization area of AMPA with NeuN-positive neurons in the PTX-Veh group ($p < 0.001$; For groups, $F_{2,\ 105} = 36.72$, $p < 0.001$), which was attenuated by vinpocetine treatment (Fig. 6F, $p = 0.0335$, colocalization coefficients are shown in Supplementary Table 1).

Collectively, these results indicate that CIPN-induced maladaptive spinal plasticity is associated with increased expression of AMPA and NR2B receptors. These alterations contribute to enhanced excitatory synaptic transmission and NMDA receptor-dependent pain sensitization.

3.7. Repeated treatment of vinpocetine regulates PKC-α expression in the spinal cord of a CIPN model

Given that vinpocetine downregulated AMPA receptor expression in CIPN, we further examined its effects on key regulators of AMPA receptor function, including PKC-α, CaMKII-α, and PKA. To assess the influence of vinpocetine on these pathways, Western blot analysis was performed on PID14 following repeated vinpocetine treatment (i.p.).

Western blot results revealed a significant upregulation of PKC-α in the PTX-Veh group compared to the Veh-Veh group (Fig. 7A, $p = 0.0053$; $F_{2,\ 15} = 9.150$, $p = 0.0025$), indicating CIPN-induced enhancement of AMPA receptor signaling. Vinpocetine treatment significantly reduced PKC-α expression in the PTX-Vin group ($p = 0.006$), suggesting its involvement in the suppression of CIPN-associated synaptic plasticity. CaMKII-α expression showed no significant differences among all groups (Fig. 7B). Similarly, PKA expression showed no significant differences among the three groups (Fig. 7C). These findings suggest that vinpocetine primarily modulates AMPA receptor function through the PKC-α pathway with limited involvement of CaMKII-α and PKA.

To further examine the spatial distribution of PKC-α expression, IHC was performed on the dorsal horn of the spinal cord. PKC-α was predominantly localized in the superficial dorsal horn (Fig. 7D), where fluorescence intensity was significantly higher in the PTX-Veh group than in the Veh-Veh group (Fig. 7E, $p < 0.001$; $F_{2,\ 123} = 18.69$, $p < 0.001$). Vinpocetine treatment significantly reduced the fluorescence intensity ($p = 0.0068$), further confirming its role in downregulating PKC-α expression. Colocalization analysis with NeuN, a neuronal marker, demonstrated that the colocalization area of PKC-α with NeuN-positive neurons was significantly elevated in the PTX-Veh group compared to that in the Veh-Veh group (Fig. 7F, $p = 0.034$; $F_{2,\ 58} = 4.684$, $p = 0.13$). Vinpocetine treatment markedly decreased PKC-α colocalization with NeuN ($p = 0.0259$), further supporting its regulatory effect on AMPA receptor signaling via the PKC-α pathway (colocalization coefficients are shown in Supplementary Table 2). These findings suggest that CIPN-induced PKC-α upregulation contributes to maladaptive synaptic plasticity and increases excitatory transmission. Vinpocetine effectively attenuates this upregulation, indicating that its analgesic effects may be mediated through the AMPA-PKC-α signaling pathway.

4. Discussion

This study explored the pain-relieving mechanisms of vinpocetine in CIPN, emphasizing its effects on oxidative stress, mitochondrial biogenesis, and central sensitization in the spinal cord. Vinpocetine effectively alleviated mechanical hypersensitivity in a paclitaxel-induced CIPN model and intrathecal administration confirmed its direct role in spinal pain modulation. Mechanistically, vinpocetine reduced mitochondrial ROS levels, restored SOD2 expression, and facilitated mitochondrial biogenesis through the PGC-1α/NRF1/TFAM signaling pathway. Additionally, it attenuated neuronal hyperactivity, downregulated AMPA and NR2B receptors, and inhibited PKC-α signaling, underscoring its impact on central sensitization. Notably, this study highlights the neuroprotective properties of vinpocetine by demonstrating its ability to enhance mitochondrial biogenesis in a CIPN model. These findings suggest a potential mechanism by which vinpocetine may alleviate neuropathic pain and counteract the neurodegenerative processes associated with CIPN.

The analgesic effects of vinpocetine were evaluated in a paclitaxel-induced CIPN model, a widely used preclinical model that closely mimics the neuropathic pain experienced by patients undergoing chemotherapy [41,42]. To determine the optimal dosing regimen, varying concentrations of vinpocetine were administered i.p. as a single dose on PID7 and PID14, followed by the assessment of mechanical hypersensitivity at these time points. A previous study showed that CIPN progresses through distinct phases, with PID7 representing the early stage and PID14 reflecting a more established neuropathic condition [42]. These phases exhibit different pain sensitivities, which can influence treatment efficacy. Comparison of these two time points allows for the evaluation of CIPN symptom progression and the assessment of whether the efficacy of vinpocetine differs between the early and late stages of the condition [5]. Behavioral assessments revealed that vinpocetine significantly alleviated mechanical hypersensitivity at both time points in a dose-dependent manner, with 20 mg/kg producing the most pronounced effect. However, its duration of action was limited to less than four hours, necessitating repeated administration to sustain efficacy. Continuous daily treatment from PID7 to PID13 significantly reduced mechanical, thermal, and cold hypersensitivity, demonstrating the need for sustained administration. DMSO was used as a vehicle for repeated intraperitoneal administration within the generally accepted safety range in mice [43]. Although DMSO is known to exhibit biological activity, particularly with repeated use [44], no abnormal behavior or

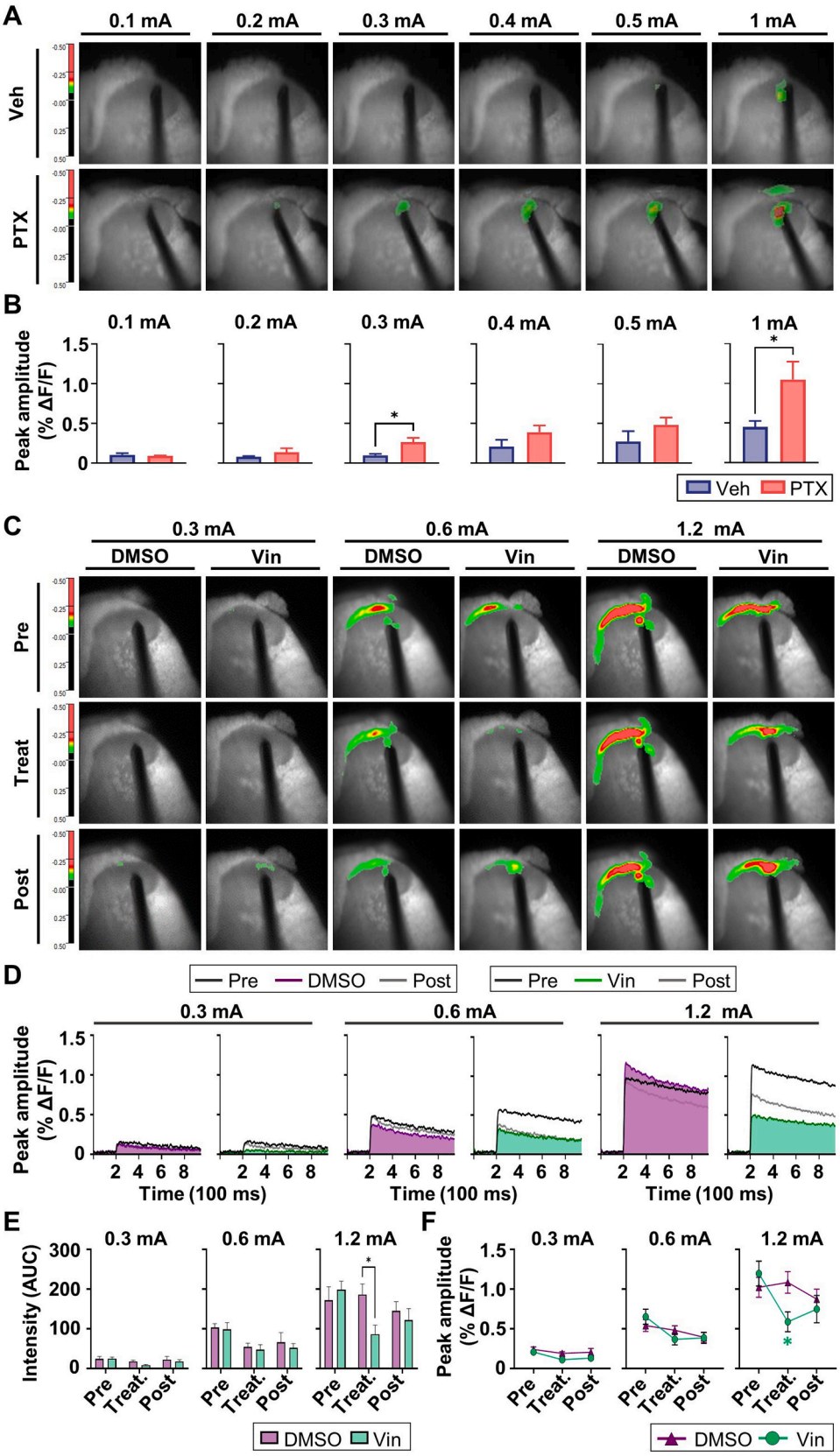

(caption on next page)

Fig. 5. Changes in neuronal activity in the spinal cord dorsal horn of the CIPN model and the inhibitory effects of vinpocetine. (A, B) Comparison of peak amplitudes between the vehicle and paclitaxel groups. (A) Representative images showing electrical stimulation intensity-dependent neuronal activity in the spinal dorsal horn of the vehicle (Veh) and paclitaxel (PTX) groups. (B) Comparison of peak amplitudes between the Veh and PTX groups at each electrical stimulation intensity (n = 6 per group). *P < 0.05, as determined using an unpaired *t*-test. (C-E) Effects of vinpocetine on neuronal activity in the spinal cord dorsal horn under different stimulation intensities in the CIPN model. (C) Representative optical images of the spinal cord in the CIPN model, comparing the DMSO and vinpocetine (Vin) groups at different stimulation intensities and phases. (D) Fluorescence responses to different stimulation intensities over time across each phase in DMSO and Vin groups (n = 9 per group). (E) Comparison of the area under the curve (AUC) from 200 ms to 943.5 ms across stimulation intensities between DMSO and Vin groups (n = 9 per group). (F) Comparison of peak amplitudes across pre-treatment, treatment, and post-treatment phases in the DMSO and Vin groups (n = 9 per group). In (E) and (F), *p < 0.05 vs. DMSO group, as determined using two-way ANOVA followed by Bonferroni's post hoc multiple comparison test.

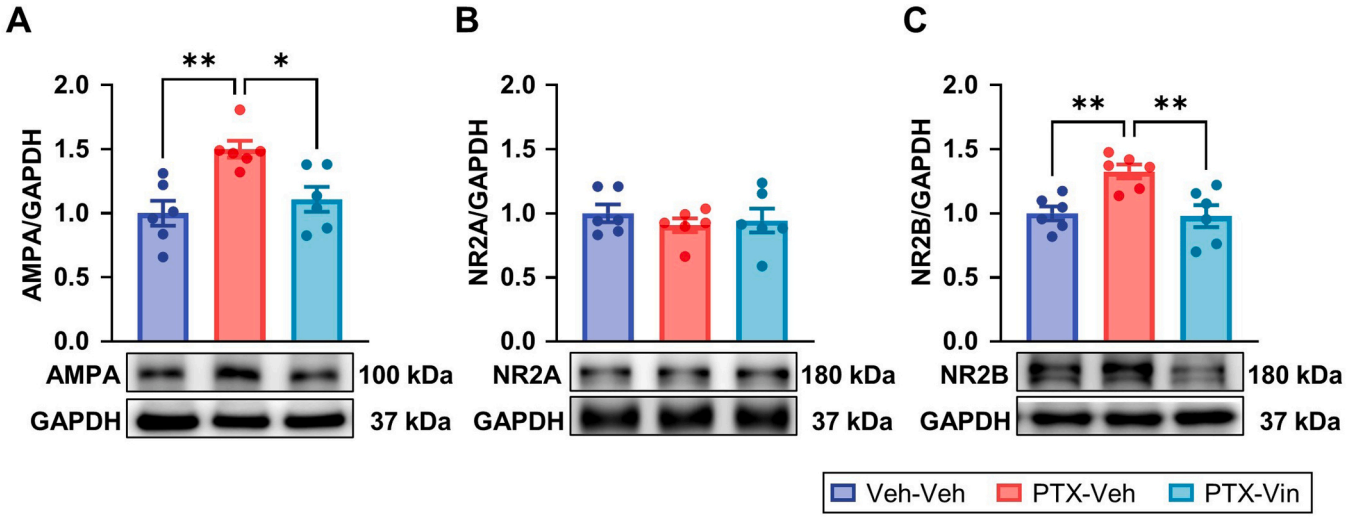

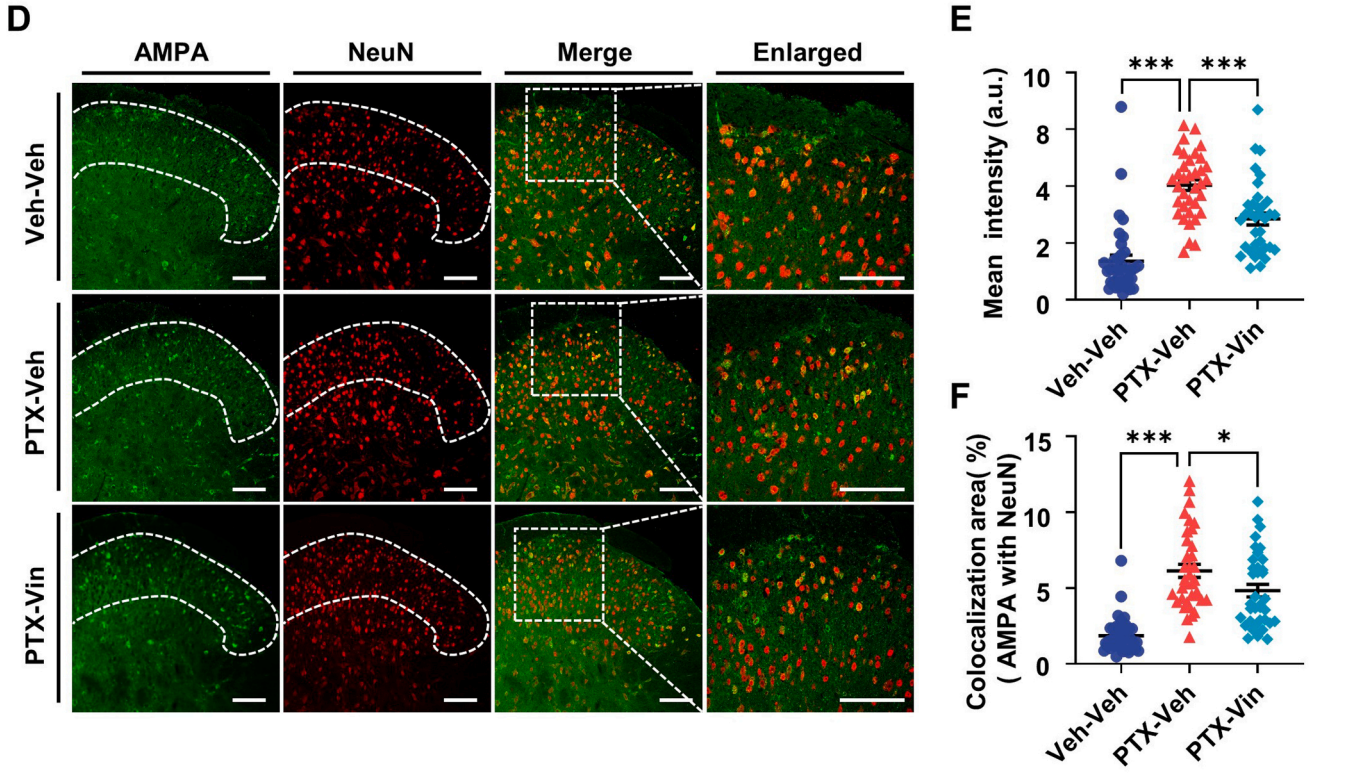

Fig. 6. Changes in central sensitization-related factors in the spinal cord dorsal horn following repeated intraperitoneal vinpocetine treatment. (A-C) Western blot analysis of the expression levels of AMPA (A), NR2A (B), and NR2B (C). The original Western blot bands are shown in Fig. S3. *p < 0.05, **p < 0.01, as determined by using one-way ANOVA followed by Tukey's post hoc multiple comparison test (n = 6 per group). (D-F) Expression of AMPA receptors in neurons in the spinal cord dorsal horn. (D) Representative confocal microscopy images of AMPA receptor (green) and NeuN (red) expression in the dorsal horn of the spinal cord from different groups. Scale bar = 100 μm. (E) Comparison of the mean fluorescence intensity of AMPA in the dorsal horn among the groups (n = 6 per group). *P < 0.05, ***p < 0.001, as determined by using one-way ANOVA followed by Tukey's post hoc multiple comparison test. (F) Comparison of the colocalization areas of AMPA and NeuN across different groups (n = 6 per group). *P < 0.05, ***p < 0.001, as determined by using one-way ANOVA followed by Tukey's post hoc multiple comparison test.

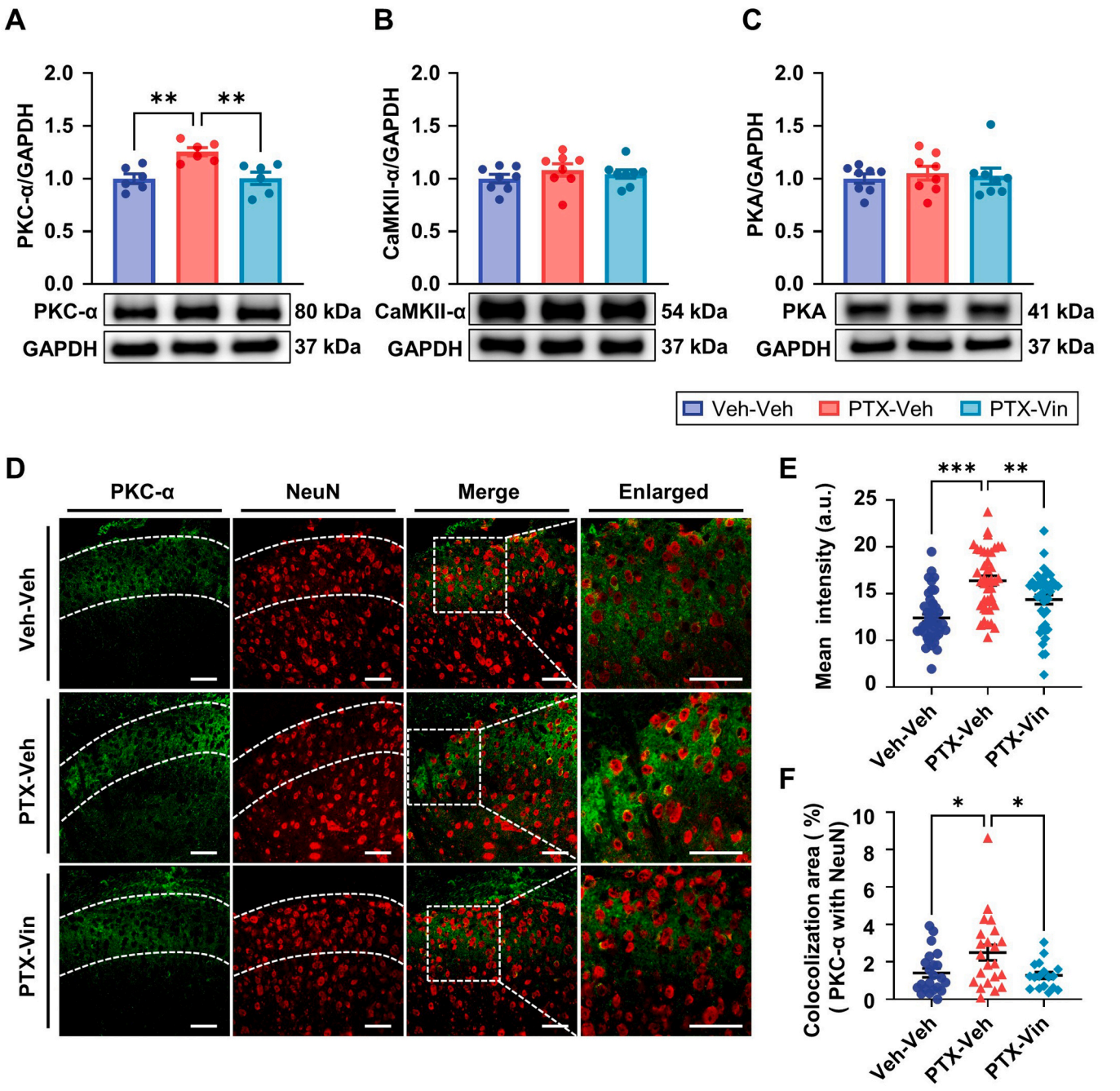

Fig. 7. Changes in kinases in the spinal cord dorsal horn following repeated intraperitoneal vinpocetine treatment. (A-C) Western blot analysis of the expression levels of PKC-α (A, n = 6 per group), CaMKII-α (B, n = 8 per group), and PKA (C, n = 8 per group). The original Western blot bands are shown in Fig. S4. $^{**}P < 0.01$, as determined by using one-way ANOVA followed by Tukey's post hoc multiple comparison test. (D-F) Expression of PKC-α with neurons in the spinal cord dorsal horn. (D) Representative confocal microscopy images of PKC-α (green) and NeuN (red) expression in the dorsal horn of the spinal cord from different groups. Scale bar = 50 μm. (E) Comparison of the mean fluorescence intensity of PKC-α in the dorsal horn among the groups (n = 6 per group). $^{**}P < 0.01$, $^{***}p < 0.001$, as determined by using one-way ANOVA followed by Tukey's post hoc multiple comparison test. (F) Comparison of the colocalization areas of PKC-α and NeuN across different groups (n = 6 per group). $^{*}P < 0.05$, $^{**}p < 0.01$, $^{***}p < 0.001$, as determined by using one-way ANOVA followed by Tukey's post hoc multiple comparison test.

adverse effects were observed in the present study. Furthermore, the absence of detectable effects in the vehicle control group, combined with the consistent use of DMSO across all experimental groups, suggests minimal risk associated with its repeated administration. Intrathecal administration of vinpocetine further confirmed its efficacy in modulating spinal cord pain. Collectively, these findings demonstrate that vinpocetine exerts significant analgesic effects in both the early and established phases of CIPN and that sustained administration is required to maintain therapeutic efficacy, with evidence pointing to its spinal involvement in the mechanism of its action.

Given the well-established role of mitochondrial dysfunction in CIPN, the potential mechanisms by which vinpocetine restores mitochondrial homeostasis were also explored. Mitochondrial dysfunction in CIPN has been linked to increased ROS production and impaired antioxidant defense mechanisms, leading to neuronal damage and heightened pain sensitivity [45,46]. MitoSOX Red staining revealed a significant reduction in mitochondrial ROS levels, suggesting a role of vinpocetine in counteracting oxidative stress-related neuropathy.

Additionally, the expression level of SOD2, a key mitochondrial antioxidant enzyme that neutralizes mitochondrial ROS [47], was upregulated, indicating enhanced mitochondrial antioxidant defense. Previous studies have suggested that mitochondrial oxidative damage can regulate SOD2 activity through post-translational modifications such as nitration or phosphorylation, which affects its stability and function [48–50]. Furthermore, decreased oxidative stress can lead to reduced demand for SOD2 expression, as cells may no longer require heightened antioxidant defense under conditions of low ROS production [51]. Further investigation is required to determine whether vinpocetine influences SOD2 expression directly or indirectly by reducing the oxidative burden. In the present study, vinpocetine alleviated oxidative stress and concurrently enhanced mitochondrial biogenesis, as indicated by the upregulation of PGC-1α, NRF1, and TFAM. PGC-1α is a key regulator of mitochondrial biogenesis, coordinating the transcription of genes essential for mitochondrial replication and function [22,52]. The upregulation of PGC-1α following vinpocetine treatment indicates enhanced mitochondrial recovery, which may improve cellular resistance to oxidative damage and support sustained neuronal function [53]. These findings indicate that vinpocetine concurrently mitigates oxidative stress and enhances mitochondrial biogenesis, thereby contributing to its therapeutic effects in CIPN.

Building on these findings, we evaluated the therapeutic potential of vinpocetine in oxidative stress-induced neuropathic pain using A.A- and KO_2-induced pain models. These agents are widely recognized for their ability to disrupt mitochondrial electron transport and exacerbate oxidative damage, thereby modeling neuropathic pain driven by oxidative stress [54,55]. In our study, intrathecal administration of vinpocetine significantly alleviated mechanical hypersensitivity in both models, reinforcing its efficacy in mitigating oxidative stress-associated pain. Considering the known role of vinpocetine as a phosphodiesterase-1 (PDE1) inhibitor, its neuroprotective effects may also stem from its ability to regulate intracellular calcium homeostasis [56–58]. These results align with previous reports highlighting the analgesic benefits of targeting oxidative stress pathways [59–61], and collectively position vinpocetine as a compelling candidate for treating neuropathic conditions beyond CIPN.

To further elucidate the mechanisms underlying the effects of vinpocetine, we assessed spinal cord excitability using VSDI in L4 spinal cord slices from CIPN models on PID14. As a real-time functional imaging technique, the VSDI enables the precise assessment of neuronal hyperexcitability associated with pain [62,63]. A stimulation threshold of 0.3 mA was chosen to detect enhanced neuronal responses in CIPN, serving as a reference point for comparisons in this study. Vinpocetine administration resulted in pronounced stimulation-dependent suppression of neuronal activity across intensities of 0.3, 0.6, 1.2 mA, with the strongest inhibition observed at 1.2 mA. These findings suggest that vinpocetine attenuates CIPN-related spinal hyperexcitability likely by dampening excessive neuronal firing and modulating central sensitization mechanisms.

Further mechanistic analyses examined excitatory synaptic receptors and intracellular signaling pathways relevant to pain processing. Western blot analysis revealed that AMPA and NR2B receptor levels were significantly downregulated following vinpocetine treatment, whereas NR2A levels remained unchanged. These findings align with previous studies that demonstrated the critical involvement of spinal AMPA receptors in both acute and persistent pain mechanisms [64,65]. In addition, vinpocetine has been reported to inhibit NaV1.8 sodium channel activity, which may further contribute to its ability to reduce neuronal excitability and pain perception [66]. Given that AMPA and NR2B receptors are key mediators of synaptic plasticity and long-term potentiation (LTP) [67], their downregulation implies that vinpocetine modulates excitatory synaptic transmission, thereby dampening pain hypersensitivity. Consistent with this, IHC analysis revealed a marked increase in the colocalization of AMPA and NeuN in the CIPN group, indicating elevated AMPA receptor expression in neurons [25]. This indicates that enhanced excitatory activity underlies the central sensitization. Vinpocetine treatment significantly reduced the colocalization area of AMPA with NeuN, further supporting its role in the attenuation of neuronal hyperexcitability. Previous studies have also demonstrated that targeting oxidative stress pathways can mitigate neuropathic pain [68,69], suggesting that the antioxidative effects of vinpocetine may play a role in the observed downregulation of excitatory synaptic components. Collectively, these results suggest that vinpocetine exerts its analgesic effects through a multifaceted mechanism involving suppression of glutamatergic transmission, inhibition of sodium channel activity [66], and modulation of oxidative stress, ultimately leading to reduced central sensitization and neuronal hyperactivity in CIPN. These findings underscore AMPA receptor modulation as a possible mechanism underlying the analgesic effect of vinpocetine [70].

In the present study, vinpocetine selectively reduced PKC-α expression, while CaMKII-α and PKA levels remained unchanged, indicating targeted modulation of protein kinase signaling. Given that vinpocetine inhibits NF-κB-dependent inflammatory signaling and directly targets IκB kinase [71], it is plausible that its effect on PKC-α contributes to the attenuation of central sensitization. Since PKC-α regulates AMPA receptor trafficking and phosphorylation [72], its downregulation is associated with decreased synaptic excitability, further reinforcing the modulatory effect of vinpocetine on excitatory transmission. Previous studies have shown that PKC-α activity enhances synaptic strength and facilitates central sensitization in pain models, highlighting its crucial role in pain plasticity [72,73]. In this context, vinpocetine-induced suppression of PKC-α reflects selective disruption of signaling pathways involved in nociceptive transmission [74]. Moreover, IHC analysis demonstrated that vinpocetine treatment reduced the colocalization of PKC-α with NeuN-positive neurons, suggesting changes in both its expression and subcellular localization. These findings indicate that vinpocetine influences PKC-α-dependent mechanisms at both the molecular and structural levels, contributing to its antinociceptive effects in CIPN. Taken together, these results support a mechanistic model in which vinpocetine restores mitochondrial biogenesis via PGC-1α/NRF1/TFAM activation, reduces ROS levels by preserving antioxidant capacity, and suppresses PKC-α-regulated excitatory transmission in the spinal cord. These actions converge to mitigate central sensitization and alleviate CIPN-related symptoms. The overall mechanism is illustrated in Fig. 8.

Nonetheless, this study has several limitations. Although we observed robust upregulation of PGC-1α, NRF1, and TFAM in conjunction with behavioral improvements, the involvement of mitochondrial biogenesis has not been directly validated using genetic or pharmacological inhibition. Thus, further investigations are required to confirm the causal role of this pathway. In addition, while the downregulation of NR2B, AMPA receptor subunits, and PKC-α suggests reduced excitatory synaptic transmission, functional validation using selective inhibitors or knockdown models has not yet been performed. Given that NR2B inhibition reverses oxaliplatin-induced mechanical allodynia [75], and PKC-α blockade attenuates pain by modulating AMPA receptor trafficking [73], functional studies would be necessary in the future. Moreover, we used only male mice to minimize variability from hormonal fluctuations, but this introduces a limitation in that the findings may not be generalizable to females, as sex differences shaped by hormonal and neuroimmune mechanisms significantly influence pain processing and CIPN susceptibility.

Future studies that incorporate both sexes and direct pathway manipulation are essential to clarify the mechanisms underlying the effects of vinpocetine. Additionally, these preclinical findings support further investigation of the translational potential of vinpocetine in the management of CIPN, including its safety, efficacy, and sex-specific effects in clinical settings.

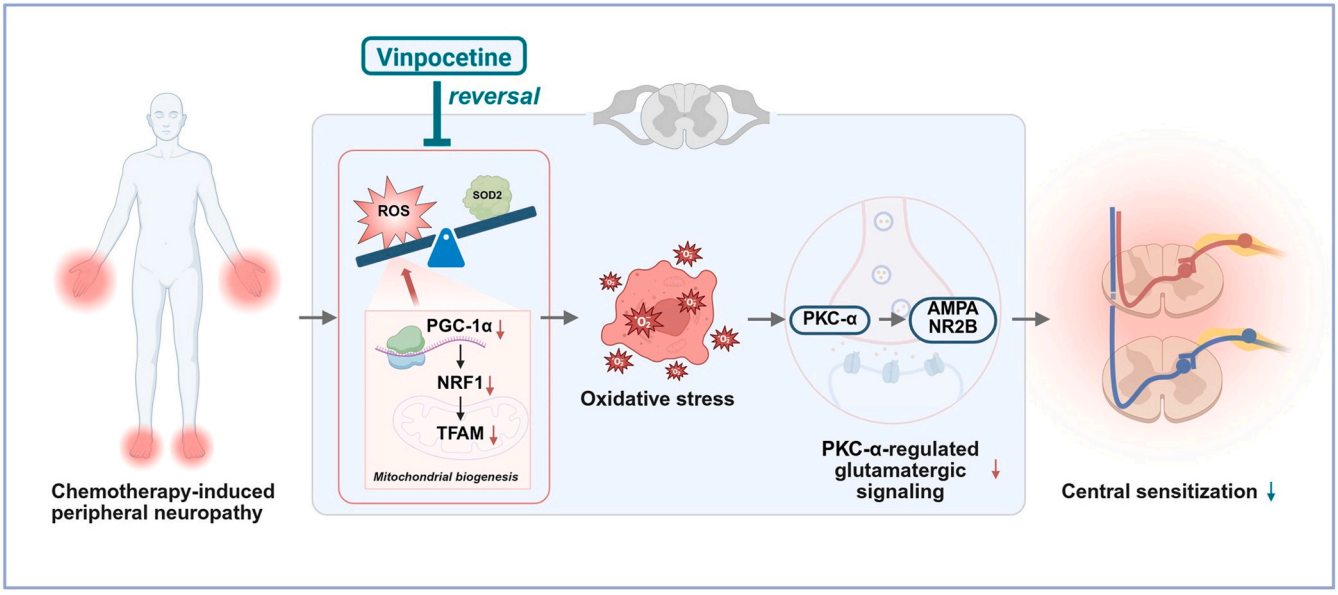

Fig. 8. Schematic summary of spinal alterations in CIPN and the modulatory effects of vinpocetine. In CIPN, downregulation of the PGC-1α/NRF1/TFAM signaling pathway, increased mitochondrial ROS, and reduced SOD2 contribute to oxidative stress, which enhances PKC-α-regulated glutamatergic signaling in the pain pathway, leading to central sensitization. Vinpocetine reverses these pathological changes by promoting mitochondrial biogenesis, reducing oxidative stress, and dampening excitatory synaptic transmission, thereby alleviating CIPN symptoms. Illustration created using BioRender (https://BioRender.com).

5. Conclusion

The findings of this study support the potential use of vinpocetine for the treatment of CIPN. Vinpocetine mitigates CIPN by targeting oxidative stress, enhancing mitochondrial biogenesis, and modulating spinal cord excitability. Notably, this study is the first to demonstrate the role of vinpocetine in promoting mitochondrial biogenesis via the PGC-1α/NRF1/TFAM pathway in a CIPN model, thus providing new insights into the mitochondrial function in pain modulation. Given the limited therapeutic options available for CIPN, this study highlights the potential of vinpocetine as a novel therapeutic strategy for CIPN and provides a foundation for future translational research aimed at improving neuropathic pain management in patients undergoing chemotherapy. However, further studies, including clinical trials, would be necessary to evaluate the safety, efficacy, and sex-specific responses of the patients to vinpocetine.

Abbreviations

A.A, antimycin A; AMPA, α-amino-3-hydroxy-5-methyl-4-isoxazolepropionic acid receptor; AUC, area under curve; CaMKII-α, calcium/calmodulin-dependent protein kinase II alpha; CIPN, chemotherapy-induced peripheral neuropathy; IHC, immunohistochemistry; KO_2, potassium superoxide; MWT, mechanical withdrawal threshold; NR2A, N-methyl-D-aspartate receptor subunit 2A; NR2B, N-methyl-D-aspartate receptor subunit 2B; NRF1,nuclear respiratory factor 1; PBN, N-tert-butyl-α-phenylnitrone; PID, post-injection day; PGC-1 α, peroxisome proliferator-activated receptor gamma coactivator-1 alpha; PKA, protein kinase A; PKC- α, protein kinase C alpha; PTX, paclitaxel; PWL, paw withdrawal latency; ROS, reactive oxygen species; TFAM,mitochondrial transcription factor A; TEMPOL, 4-hydroxy-2,2,6,6-tetramethylpiperidine-1-oxyl; VSDI, voltage-sensitive dye imaging.

CRediT authorship contribution statement

Guanghai Nan: Writing – original draft, Visualization, Investigation, Methodology, Data curation. **Lin Lin:** Methodology, Data curation, Validation. **Leejeong Kim:** Methodology, Data curation. **Kyeongmin Kim:** Methodology, Data curation. **Nari Kang:** Methodology, Data curation. **Hee Young Kim:** Methodology, Investigation. **Myeounghoon Cha:** Supervision, Conceptualization, Funding acquisition. **Bae Hwan Lee:** Supervision, Conceptualization, Funding acquisition.

Funding

This study was supported by National Research Foundation of Korea (NRF) grants funded by the Korean government (MSIT) (NRF-2020R1A2C3008481 and RS-2023-00238538) and Soonchunhyang University Research Fund (20250563).

Declaration of Competing Interest

The authors declare that they have no known competing financial interests or personal relationships that could have appeared to influence the work reported in this paper.

Acknowledgement

We would like to thank Medical Illustration & Design (MID), a member of the Medical Research Support Services of Yonsei University College of Medicine, for providing excellent support with medical illustrations.

Appendix A. Supporting information

Supplementary data associated with this article can be found in the online version at doi:10.1016/j.biopha.2025.118434.

Data availability

No data was used for the research described in the article.

References

[1] E.H. Bae, M.K. Greenwald, A.G. Schwartz, Chemotherapy-induced peripheral neuropathy: mechanisms and therapeutic avenues, Neurotherapeutics 18 (4) (2021) 2384–2396.
[2] J. Addington, M. Freimer, Chemotherapy-induced peripheral neuropathy: an update on the current understanding, F1000Res 5 (2016).
[3] M. Seretny, G.L. Currie, E.S. Sena, S. Ramnarine, R. Grant, M.R. MacLeod, L. A. Colvin, M. Fallon, Incidence, prevalence, and predictors of chemotherapy-induced peripheral neuropathy: a systematic review and meta-analysis, Pain 155 (12) (2014) 2461–2470.
[4] E.Y. Ibrahim, B.E. Ehrlich, Prevention of chemotherapy-induced peripheral neuropathy: a review of recent findings, Crit. Rev. Oncol. Hematol. 145 (2020) 102831.
[5] S.J.L. Flatters, P.M. Dougherty, L.A. Colvin, Clinical and preclinical perspectives on chemotherapy-induced peripheral neuropathy (CIPN): a narrative review, Br. J. Anaesth. 119 (4) (2017) 737–749.
[6] A. Shah, E.M. Hoffman, M.L. Mauermann, C.L. Loprinzi, A.J. Windebank, C. J. Klein, N.P. Staff, Incidence and disease burden of chemotherapy-induced peripheral neuropathy in a population-based cohort, J. Neurol. Neurosurg. Psychiatry 89 (6) (2018) 636–641.
[7] C.T. Pike, H.G. Birnbaum, C.E. Muehlenbein, G.M. Pohl, R.B. Natale, Healthcare costs and workloss burden of patients with chemotherapy-associated peripheral neuropathy in breast, ovarian, head and neck, and nonsmall cell lung cancer, Chemother. Res. Pr. 2012 (1) (2012) 913848.
[8] A.D. Desforges, C.M. Hebert, A.L. Spence, B. Reid, H.A. Dhaibar, D. Cruz-Topete, E. M. Cornett, A.D. Kaye, I. Urits, O. Viswanath, Treatment and diagnosis of chemotherapy-induced peripheral neuropathy: an update, Biomed. Pharm. 147 (2022) 112671.
[9] J.N. Mezzanotte, M. Grimm, N.V. Shinde, T. Nolan, L. Worthen-Chaudhari, N. O. Williams, M.B. Lustberg, Updates in the treatment of chemotherapy-induced peripheral neuropathy, Curr. Treat. Options Oncol. 23 (1) (2022) 29–42.
[10] A.A. Argyriou, J. Bruna, S.B. Park, G. Cavaletti, Emerging pharmacological strategies for the management of chemotherapy-induced peripheral neurotoxicity (CIPN), based on novel CIPN mechanisms, Expert Rev. Neurother. 20 (10) (2020) 1005–1016.
[11] J. Gu, M. Hu, Z. Gu, J. Yu, Y. Ji, L. Li, C. Hu, G. Wei, J. Huo, Bibliometric analysis reveals a 20-year research trend for chemotherapy-induced peripheral neuropathy, Front Neurol. 12 (2021) 793663.
[12] H. Starobova, I. Vetter, Pathophysiology of chemotherapy-induced peripheral neuropathy, Front Mol. Neurosci. 10 (2017) 174.
[13] A. Canta, E. Pozzi, V.A. Carozzi, Mitochondrial dysfunction in chemotherapy-induced peripheral neuropathy (CIPN), Toxics 3 (2) (2015) 198–223.
[14] A. Areti, V.G. Yerra, V. Naidu, A. Kumar, Oxidative stress and nerve damage: role in chemotherapy induced peripheral neuropathy, Redox Biol. 2 (2014) 289–295.
[15] C. Guo, L. Sun, X. Chen, D. Zhang, Oxidative stress, mitochondrial damage and neurodegenerative diseases, Neural Regen. Res 8 (21) (2013) 2003–2014.
[16] H. Tirichen, H. Yaigoub, W. Xu, C. Wu, R. Li, Y. Li, Mitochondrial reactive oxygen species and their contribution in chronic kidney disease progression through oxidative stress, Front Physiol. 12 (2021) 627837.
[17] A. Trecarichi, S.J.L. Flatters, Mitochondrial dysfunction in the pathogenesis of chemotherapy-induced peripheral neuropathy, Int Rev. Neurobiol. 145 (2019) 83–126.
[18] M. Waseem, P. Kaushik, H. Tabassum, S. Parvez, Role of mitochondrial mechanism in chemotherapy-induced peripheral neuropathy, Curr. Drug Metab. 19 (1) (2018) 47–54.
[19] H.S. Shim, C. Bae, J. Wang, K.H. Lee, K.M. Hankerd, H.K. Kim, J.M. Chung, J.H. La, Peripheral and central oxidative stress in chemotherapy-induced neuropathic pain, Mol. Pain. 15 (2019) 1744806919840098.
[20] N.A. Duggett, L.A. Griffiths, S.J.L. Flatters, Paclitaxel-induced painful neuropathy is associated with changes in mitochondrial bioenergetics, glycolysis, and an energy deficit in dorsal root ganglia neurons, Pain 158 (8) (2017) 1499–1508.
[21] S.D. Chen, D.I. Yang, T.K. Lin, F.Z. Shaw, C.W. Liou, Y.C. Chuang, Roles of oxidative stress, apoptosis, PGC-1alpha and mitochondrial biogenesis in cerebral ischemia, Int J. Mol. Sci. 12 (10) (2011) 7199–7215.
[22] P.A. Li, X. Hou, S. Hao, Mitochondrial biogenesis in neurodegeneration, J. Neurosci. Res 95 (10) (2017) 2025–2029.
[23] M. Fontecha-Barriuso, D. Martin-Sanchez, J.M. Martinez-Moreno, M. Monsalve, A. M. Ramos, M.D. Sanchez-Nino, M. Ruiz-Ortega, A. Ortiz, A.B. Sanz, The role of PGC-1alpha and mitochondrial biogenesis in kidney diseases, Biomolecules 10 (2) (2020).
[24] C. Bouchez, A. Devin, Mitochondrial biogenesis and mitochondrial reactive oxygen species (ROS): a complex relationship regulated by the cAMP/PKA signaling pathway, Cells 8 (4) (2019).
[25] A. Latremoliere, C.J. Woolf, Central sensitization: a generator of pain hypersensitivity by central neural plasticity, J. Pain. 10 (9) (2009) 895–926.
[26] N. Chen, M.M. Ge, D.Y. Li, X.M. Wang, D.Q. Liu, D.W. Ye, Y.K. Tian, Y.Q. Zhou, J. P. Chen, beta2-adrenoreceptor agonist ameliorates mechanical allodynia in paclitaxel-induced neuropathic pain via induction of mitochondrial biogenesis, Biomed. Pharm. 144 (2021) 112331.
[27] M. Fidanboylu, L.A. Griffiths, S.J. Flatters, Global inhibition of reactive oxygen species (ROS) inhibits paclitaxel-induced painful peripheral neuropathy, PLoS One 6 (9) (2011) e25212.
[28] S.E. Park, C. Neupane, C. Noh, R. Sharma, H.J. Shin, T.L. Pham, G.S. Lee, K.D. Park, C.J. Lee, D.W. Kang, S.Y. Lee, H.W. Kim, J.B. Park, Antiallodynic effects of KDS2010, a novel MAO-B inhibitor, via ROS-GABA inhibitory transmission in a paclitaxel-induced tactile hypersensitivity model, Mol. Brain 15 (1) (2022) 41.
[29] H.M. Al-Kuraishy, A.I. Al-Gareeb, M.T. Naji, F. Al-Mamorry, Role of vinpocetine in ischemic stroke and poststroke outcomes: a critical review, Brain Circ. 6 (1) (2020) 1–10.
[30] J. Sheng, S. Zhang, L. Wu, G. Kumar, Y. Liao, P. Gk, H. Fan, Inhibition of phosphodiesterase: a novel therapeutic target for the treatment of mild cognitive impairment and alzheimer's disease, Front Aging Neurosci. 14 (2022) 1019187.
[31] C. Pereira, P. Agostinho, P.I. Moreira, A.I. Duarte, M.S. Santos, C.R. Oliveira, Neuroprotection strategies: effect of vinpocetine in vitro oxidative stress models, Acta Med Port. 16 (6) (2003) 401–406.
[32] K. Bagri, R. Deshmukh, Vinpocetine restores cognitive and motor functions in traumatic brain injury challenged rats, Inflammopharmacology 30 (6) (2022) 2243–2259.
[33] Y. Lourenco-Gonzalez, V. Fattori, T.P. Domiciano, A.C. Rossaneis, S.M. Borghi, T. H. Zaninelli, C. Bernardy, J.C. Alves-Filho, T.M. Cunha, F.Q. Cunha, R. Casagrande, W.A. Verri, Repurposing of the nootropic drug vinpocetine as an analgesic and anti-inflammatory agent: evidence in a mouse model of superoxide anion-triggered inflammation, Mediat. Inflamm. 2019 2019 (2019), 6481812-14.
[34] O.M.Abdel Salam, Vinpocetine and piracetam exert antinociceptive effect in visceral pain model in mice, Pharm. Rep. 58 (5) (2006) 680–691.
[35] G. Svab, J. Doczi, A.A. Gerencser, A. Ambrus, F. Gallyas, B. Sümegi, L. Tretter, The mitochondrial targets of neuroprotective drug vinpocetine on primary neuron cultures, brain capillary endothelial cells, synaptosomes, and brain mitochondria, Neurochem. Res 44 (10) (2019) 2435–2447.
[36] K.W. Ruiz-Miyazawa, F.A. Pinho-Ribeiro, A.C. Zarpelon, L. Staurengo-Ferrari, R. L. Silva, J.C. Alves-Filho, T.M. Cunha, F.Q. Cunha, R. Casagrande, W.A. Verri, Vinpocetine reduces lipopolysaccharide-induced inflammatory pain and neutrophil recruitment in mice by targeting oxidative stress, cytokines and NF-κB, Chem. Biol. Interact. 237 (2015) 9–17.
[37] H.Y. Kim, J.M. Chung, K. Chung, Increased production of mitochondrial superoxide in the spinal cord induces pain behaviors in mice: the effect of mitochondrial electron transport complex inhibitors, Neurosci. Lett. 447 (1) (2008) 87–91.
[38] L. Kim, G. Nan, H.Y. Kim, M. Cha, B.H. Lee, Modulation of chemotherapy-induced peripheral neuropathy by JZL195 through glia and the endocannabinoid system, Biomed. Pharmacother. 180 (2024) 117515.
[39] W. You, K. Knoops, T. Berendschot, B.J. Benedikter, C.A.B. Webers, C.P. M. Reutelingsperger, T. Gorgels, PGC-1a mediated mitochondrial biogenesis promotes recovery and survival of neuronal cells from cellular degeneration, Cell Death Discov. 10 (1) (2024) 180.
[40] Y. Zong, H. Li, P. Liao, L. Chen, Y. Pan, Y. Zheng, C. Zhang, D. Liu, M. Zheng, J. Gao, Mitochondrial dysfunction: mechanisms and advances in therapy, Signal Transduct. Target Ther. 9 (1) (2024) 124.
[41] C. Bacalhau, J.T. Costa-Pereira, I. Tavares, Preclinical research in paclitaxel-induced neuropathic pain: a systematic review, Front Vet. Sci. 10 (2023) 1264668.
[42] I. Klein, H.C. Lehmann, Pathomechanisms of paclitaxel-induced peripheral neuropathy, Toxics 9 (10) (2021) 229.
[43] M. Matias, S. Silvestre, A. Falcão, G. Alves, Considerations and pitfalls in selecting the drug vehicles for evaluation of new drug candidates: focus on in vivo pharmaco-toxicological assays based on the rotarod performance test, J. Pharm. Pharm. Sci. 21 (1) (2018) 110–118.
[44] T. Kelava, I. Ćavar, F. Čulo, Biological actions of drug solvents, Period. Biol. 113 (3) (2011) 311–320.
[45] T.M. Doyle, D. Salvemini, Mini-Review: mitochondrial dysfunction and chemotherapy-induced neuropathic pain, Neurosci. Lett. 760 (2021) 136087.
[46] E.S. Schwartz, H.Y. Kim, J. Wang, I. Lee, E. Klann, J.M. Chung, K. Chung, Persistent pain is dependent on spinal mitochondrial antioxidant levels, J. Neurosci. 29 (1) (2009) 159–168.
[47] J.M. Flynn, S. Melov, SOD2 in mitochondrial dysfunction and neurodegeneration, Free Radic. Biol. Med 62 (2013) 4–12.
[48] L. Miao, D.K. Clair St, Regulation of superoxide dismutase genes: implications in disease, Free Radic. Biol. Med 47 (4) (2009) 344–356.
[49] D. Candas, J.J. Li, MnSOD in oxidative stress response-potential regulation via mitochondrial protein influx, Antioxid. Redox Signal 20 (10) (2014) 1599–1617.
[50] J. He, X. Liu, C. Su, F. Wu, J. Sun, J. Zhang, X. Yang, C. Zhang, Z. Zhou, X. Zhang, X. Lin, J. Tao, Inhibition of mitochondrial oxidative damage improves reendothelialization capacity of endothelial progenitor cells via SIRT3 (Sirtuin 3)-enhanced SOD2 (Superoxide dismutase 2) deacetylation in hypertension, Arterioscler. Thromb. Vasc. Biol. 39 (8) (2019) 1682–1698.
[51] S. Yang, G. Lian, ROS and diseases: role in metabolism and energy supply, Mol. Cell Biochem 467 (1-2) (2020) 1–12.
[52] L. Qian, Y. Zhu, C. Deng, Z. Liang, J. Chen, Y. Chen, X. Wang, Y. Liu, Y. Tian, Y. Yang, Peroxisome proliferator-activated receptor gamma coactivator-1 (PGC-1) family in physiological and pathophysiological process and diseases, Signal Transduct. Target Ther. 9 (1) (2024) 50.
[53] S. Rius-Pérez, I. Torres-Cuevas, I. Millán, L. Ortega Á, S. Pérez, PGC-1α, inflammation, and oxidative stress: an integrative view in metabolism, Oxid. Med Cell Longev. 2020 2020 (2020) 1452696.
[54] K.R. Stanford, S.H. Hadley, I. Barannikov, J.M. Ajmo, P.K. Bahia, T.E. Taylor-Clark, Antimycin A-induced mitochondrial dysfunction activates vagal sensory neurons via ROS-dependent activation of TRPA1 and ROS-independent activation of TRPV1, Brain Res 1715 (2019) 94–105.
[55] N.A. Maioli, A.C. Zarpelon, S.S. Mizokami, C. Calixto-Campos, C. Guazelli, M. Hohmann, F.A. Pinho-Ribeiro, T.T. Carvalho, M.F. Manchope, C.R. Ferraz, R. Casagrande, W.A. Verri Jr, The superoxide anion donor, potassium superoxide,

induces pain and inflammation in mice through production of reactive oxygen species and cyclooxygenase-2, Braz. J. Med. Biol. Res. 0 (2015) 321–331.
[56] R. Deshmukh, V. Sharma, S. Mehan, N. Sharma, K.L. Bedi, Amelioration of intracerebroventricular streptozotocin induced cognitive dysfunction and oxidative stress by vinpocetine - a PDE1 inhibitor, Eur. J. Pharm. 620 (1-3) (2009) 49–56.
[57] X. Chen, C. Guo, J. Kong, Oxidative stress in neurodegenerative diseases, Neural Regen. Res 7 (5) (2012) 376–385.
[58] G. Cenini, A. Lloret, R. Cascella, Oxidative stress in neurodegenerative diseases: from a mitochondrial point of view, Oxid. Med Cell Longev. 2019 2019 (2019) 2105607.
[59] M. Zhao, X. Zhang, X. Tao, B. Zhang, C. Sun, P. Wang, T. Song, Sirt2 in the spinal cord regulates chronic neuropathic pain through Nrf2-mediated oxidative stress pathway in rats, Front Pharm. 12 (2021) 646477.
[60] J. Yowtak, K.Y. Lee, H.Y. Kim, J. Wang, H.K. Kim, K. Chung, J.M. Chung, Reactive oxygen species contribute to neuropathic pain by reducing spinal GABA release, Pain 152 (4) (2011) 844–852.
[61] S. Li, X. Li, X. Xie, X. Wei, C. Yu, C.W. Cheung, Z. Xia, G. Tian, N-Acetylcysteine attenuates hyperalgesia in rats with diabetic neuropathic pain: role of oxidative stress and inflammatory mediators and CXCR4, J. Diabetes Res 2021 (1) (2021), 8862910-10.
[62] G.C. Carlson, D.A. Coulter, In vitro functional imaging in brain slices using fast voltage-sensitive dye imaging combined with whole-cell patch recording, Nat. Protoc. 3 (2) (2008) 249–255.
[63] K. Kim, G. Nan, H. Bak, H.Y. Kim, J. Kim, M. Cha, B.H. Lee, Insular cortex stimulation alleviates neuropathic pain through changes in the expression of collapsin response mediator protein 2 involved in synaptic plasticity, Neurobiol. Dis. 194 (2024) 106466.
[64] Y. Wang, J. Wu, Z. Wu, Q. Lin, Y. Yue, L. Fang, Regulation of AMPA receptors in spinal nociception, Mol. Pain. 6 (2010) 5.
[65] O. Kopach, N. Voitenko, Spinal AMPA receptors: amenable players in central sensitization for chronic pain therapy? Channels (Austin) 15 (1) (2021) 284–297.
[66] X. Zhou, X.W. Dong, J. Crona, M. Maguire, T. Priestley, Vinpocetine is a potent blocker of rat NaV1.8 tetrodotoxin-resistant sodium channels, J. Pharm. Exp. Ther. 306 (2) (2003) 498–504.
[67] X.H. Li, H.H. Miao, M. Zhuo, NMDA receptor dependent long-term potentiation in chronic pain, Neurochem. Res 44 (3) (2019) 531–538.
[68] L. Teixeira-Santos, A. Albino-Teixeira, D. Pinho, Neuroinflammation, oxidative stress and their interplay in neuropathic pain: focus on specialized pro-resolving mediators and NADPH oxidase inhibitors as potential therapeutic strategies, Pharm. Res 162 (2020) 105280.
[69] B. Li, K. Yu, X. Zhou, J. Sun, L. Qi, W. Li, T. Yang, W. Li, N. Wang, X. Gu, S. Cui, R. Cao, Increased TSPO alleviates neuropathic pain by preventing pyroptosis via the AMPK-PGC-1α pathway, J. Headache Pain. 26 (1) (2025) 16.
[70] W. Chen, X. Dong, Y. Wang, C. Ma, AMPA receptor trafficking and pain plasticity, Neurosci. Bull. 30 (6) (2014) 973–984.
[71] K.I. Jeon, X. Xu, T. Aizawa, J.H. Lim, H. Jono, D.S. Kwon, J. Abe, B.C. Berk, J.D. Li, C. Yan, Vinpocetine inhibits NF-kappaB-dependent inflammation via an IKK-dependent but PDE-independent mechanism, Proc. Natl. Acad. Sci. USA 107 (21) (2010) 9795–9800.
[72] O. Kopach, V. Viatchenko-Karpinski, F.E. Atianjoh, P. Belan, Y.X. Tao, N. Voitenko, PKCα is required for inflammation-induced trafficking of extrasynaptic AMPA receptors in tonically firing lamina II dorsal horn neurons during the maintenance of persistent inflammatory pain, J. Pain. 14 (2) (2013) 182–192.
[73] O. Kopach, V. Krotov, A. Shysh, A. Sotnic, V. Viatchenko-Karpinski, V. Dosenko, N. Voitenko, Spinal PKCα inhibition and gene-silencing for pain relief: AMPAR trafficking at the synapses between primary afferents and sensory interneurons, Sci. Rep. 8 (1) (2018) 10285.
[74] Y. He, Z.J. Wang, Spinal and afferent PKC signaling mechanisms that mediate chronic pain in sickle cell disease, Neurosci. Lett. 706 (2019) 56–60.
[75] Y. Mihara, N. Egashira, H. Sada, T. Kawashiri, S. Ushio, T. Yano, H. Ikesue, R. Oishi, Involvement of spinal NR2B-containing NMDA receptors in oxaliplatin-induced mechanical allodynia in rats, Mol. Pain. 7 (2011) 8.